J. Nonlinear Sci. Vol. 15: pp. 255–289 (2005)
DOI: 10.1007/s00332-004-0650-9

Journal of
Nonlinear
Science

Locomotion of Articulated Bodies in a Perfect Fluid

E. Kanso,[1] J. E. Marsden,[1] C. W. Rowley,[2] and J. B. Melli-Huber[2]

[1] Control and Dynamical Systems, California Institute of Technology, Mail stop: CDS107-81, Pasadena, CA 91125, USA

[2] Mechanical and Aerospace Engineering, Princeton University, D232 Engineering Quad, Princeton, NJ 08544, USA

Received June 20, 2004; revised March 7, 2005; revision accepted April 9, 2005
Online publication August 5, 2005
Communicated by P. K. Newton

Summary. This paper is concerned with modeling the dynamics of N articulated solid bodies submerged in an ideal fluid. The model is used to analyze the locomotion of aquatic animals due to the coupling between their shape changes and the fluid dynamics in their environment.

The equations of motion are obtained by making use of a two-stage reduction process which leads to significant mathematical and computational simplifications. The first reduction exploits particle relabeling symmetry: that is, the symmetry associated with the conservation of circulation for ideal, incompressible fluids. As a result, the equations of motion for the submerged solid bodies can be formulated without explicitly incorporating the fluid variables. This reduction by the fluid variables is a key difference with earlier methods, and it is appropriate since one is mainly interested in the location of the bodies, not the fluid particles.

The second reduction is associated with the invariance of the dynamics under superimposed rigid motions. This invariance corresponds to the conservation of total momentum of the solid-fluid system. Due to this symmetry, the net locomotion of the solid system is realized as the sum of geometric and dynamic phases over the shape space consisting of allowable relative motions, or deformations, of the solids. In particular, reconstruction equations that govern the net locomotion at zero momentum, that is, the geometric phases, are obtained.

As an illustrative example, a planar three-link mechanism is shown to propel and steer itself at zero momentum by periodically changing its shape. Two solutions are presented: one corresponds to a hydrodynamically decoupled mechanism and one is based on accurately computing the added inertias using a boundary element method. The hydrodynamically decoupled model produces smaller net motion than the more accurate model, indicating that it is important to consider the hydrodynamic interaction of the links.

Key words. Locomotion, perfect fluid, Lagrangian, principal bundle, connection

1. Introduction

This paper formulates the equations governing the motion of a system of solid bodies that can change their shape and are submerged in an ideal fluid. The primary motivation behind this formulation is to study the dynamics of aquatic animals—more specifically, the way in which they propel and steer themselves by coupling their shape changes to the surrounding fluid dynamics.

History and Setting of the Problem. Understanding the dynamics of swimming has intrigued researchers for a long time. Early efforts in this field can be traced back to the work of Giovanni Borelli's [1989] *On the Movement of Animals*, which was first published in 1680 and 1681. Nowadays, one finds a large body of literature that addresses the swimming of fish, both from biological and biomechanic aspects. We mention, for example, the work of Wu [1971], Lighthill [1975], and Newman and Wu [1975] for their significant contributions to the understanding of the biomechanics of swimming. Besides the interest in understanding the swimming of marine animals, researchers have studied the efficiency, maneuverability, and stealth of these animals, which have provided an attractive example for designing biomimetic robots. Indeed, serious efforts have emerged in the past few years to study, build, and control underwater vehicles that move and steer by *changes of shape*, and not by direct propulsion, such as with propellers; see, for example, Mason and Burdick [2000], Morgansen, Duindam, Mason, Burdick, and Murray [2001], Kelly [1998], and Radford [2003].

The formulation presented in this paper is most suited for the analysis of aquatic animals whose propulsive movements are analogous to the movements of carangiform and thunniform fish. Carangiform fish are characterized by large, high-aspect-ratio tails, and swim mostly by moving their tails while keeping the rest of their body fairly rigid. A biological fish can regulate its buoyancy and remains approximately neutrally buoyant when swimming in a plane perpendicular to the direction of gravity. Hence, it is a reasonable first step to model the fish as a system of neutrally buoyant, articulated solid bodies.

Swimming in Potential Flow. We consider the case of potential flow to discern the fundamental principles of fish locomotion. Under these idealized conditions, that is, *in the absence of a vortex-shedding mechanism*, we show that a fish modeled as an articulated system of rigid links can propel and steer itself by controlling its shape variables (the allowable relative rotations between the links). This result is important because, contrary to the common belief, it demonstrates that the forces and moments applied on the fish body by shed vortices are *not solely* responsible for the net locomotion. The net locomotion in potential flow occurs due to the transfer of momentum between the articulated body and the fluid. Starting from rest, the articulated body changes its shape by applying internal torques at its joints. This shape actuation sets the surrounding fluid into motion, and the coupling between the shape dynamics and the surrounding fluid causes the net locomotion of the articulated solid. If the applied torques are then set to zero, the solid and fluid remain in motion by continuity, and their dynamics afterwards is described as an initial value problem. However, if the shape actuation is stopped in such a way as to lock the shape of the articulated body, in this case both the solid and

fluid motions become still. Clearly, to lock its shape, the body needs to apply torques at its joints to prevent them from moving in reaction to the surrounding fluid—that is, the body generates *a finite amount of work* that *balances the work previously done* and causes the motion of the system to stop dead.

The Role of Vorticity. Fish in nature, however, do interact with vortices shed by the fish itself or generated by other moving organisms or fixed obstacles (see, for example, Webb [1991]). Recent works provide experimental evidence which shows that fish swimming in such natural environments often prefer to exploit the circulation in the flow to reduce locomotory costs; see, for example, Müller [2003], Liao, Beal, Lauder, and Triantafyllou [2003a], and Liao, Beal, Lauder, and Triantafyllou [2003b]. Therefore, understanding how fish behave in the presence of vortices is essential in studying aquatic propulsion and stability. For this reason, we view the present study, that is, swimming in a potential flow with zero circulation, as the first step in the generation of a family of models that will eventually treat the interaction of the fish with self-generated vortices as well as with vortices shed by other objects; see Figure 1. We expect that recent models of bodies interacting dynamically with vortices, such as those of Shashikanth, Marsden, Burdick, and Kelly [2002] and Borisov and Mamaev [2003], will also be useful in our

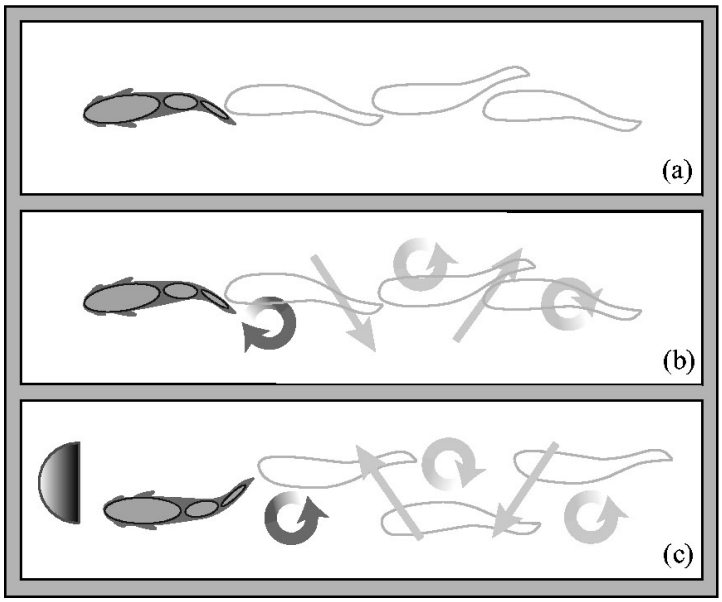

Fig. 1. (a) Fish swimming in an infinite potential flow. The body of the fish is modeled as a system of articulated solid bodies. (b) Vortices shed by a swimming fish, the brighter vortices being the most recent. The vortices form a thrust wake, that is, a wake that resembles drag wakes generated behind stationary obstacles but with opposite direction of rotation. (c) Fish swimming in a drag wake generated behind a solid obstacle. The undulating fish weaves through the vortex street as if it were generating a thrust wake. Figure inspired by Müller [2003].

future studies. Such theoretical and computational models will complement the recent experimental and empirical studies on the wake dynamics and its interaction with the shape kinematics of biological fish, as done in Tytell and Lauder [2004] and Tytell [2004] in the case of an eel swimming.

Particle Relabeling Symmetry of the Fluid. A reduced formulation of the dynamics of the solid bodies that does not *explicitly incorporate the ambient fluid* is derived. The underlying assumption is that the motion of the solids does not generate circulation. In this case, Kelvin's circulation theorem states that the circulation remains constant around any closed material contour moving with the fluid; see, for example, Chorin and Marsden [1979] for proofs and discussion. Physically, this happens because no shear stresses act within the fluid. Thus, an initially potential (irrotational) flow remains potential throughout the motion. By the same token, starting at a nonzero vorticity, the conservation of circulation is equivalent to vorticity advection.

In the geometric mechanics approach to fluid mechanics, this conservation law corresponds to the symmetry of the system under the action of the group of invertible volume-preserving mappings, discussed in more detail in Section 2. We use this symmetry and techniques from reduction theory to eliminate the fluid variables in the case of potential flow and identify the reduced configuration space with the configuration space $\mathcal{R}$ of the submerged solids. The Lagrangian of the system is then expressed as a function on the phase space $T\mathcal{R}$. The effect of the fluid is accounted for by the added inertias to the submerged bodies. We give explicit expressions for the added inertias as boundary integral functions of the fluid density and velocity potentials, consistent with the expressions given by Kirchhoff; see Lamb [1932, Chapter 6]. These potentials are functions of the configuration of the submerged bodies and are computed at the solid boundaries using a boundary element method in Section 7. It is worth noting that, in the case of rotational flow such as in the presence of point vortices, the reduced configuration space is not identifiable with $\mathcal{R}$. The reduction process for this case will be discussed in a future work. We also note that the dynamics of articulated bodies moving in an ideal, incompressible fluid has been studied in Radford [2003] without eliminating the fluid variables, and this leads to a more complex theory.

Symmetry under Superimposed Rigid Motions. The dynamics of the solid and fluid system is invariant under superimposed rigid motions. This invariance corresponds to a symmetry, namely, the conservation of total momentum of the solid-fluid system, and can be exploited to describe the dynamics on a properly defined, reduced phase space. In this formulation, the net locomotion of the articulated body in the ambient fluid is described by *vertical* Lagrange's equations, coupled, via the shape variables, to *horizontal* equations that govern the shape motion. The advantages of such a formulation is that it allows one to think of the net motion as a sum of geometric and dynamic phases over closed curves in the shape space. In particular, at zero momentum, the net locomotion is due to only geometric phases, or holonomy. We discuss this case and provide expressions for the reconstruction equations of the net motion. If one likes, this approach may be viewed as an example in the theory of *reduction by stages* when one has two symmetry groups in a problem; see Marsden, Misiolek, Ortega, Perlmutter, and Ratiu [2004].

Organization of the Paper. First, Section 2 describes the general setting of the problem and argues that, for potential flows, the dynamics of the system consisting of the bodies together with the fluid can be studied on $T\mathcal{R}$. In Section 3, there is a derivation of an expression for the Lagrangian function on $T\mathcal{R}$ together with a definition of the added inertia matrices. The structure of the configuration space $\mathcal{R}$ as a principal bundle over the shape space of allowable relative motions of the solid bodies is discussed in Section 4. The reduced dynamics is then formulated using Lagrange's equations in Section 5. The reconstruction equation for the net locomotion as a function of the shape variables are derived in Section 6. The motion of a planar three-link mechanism at zero momentum is studied in Section 7.

2. Problem Description

We study the dynamics and locomotion of a collection of bodies that can undergo shape changes and are immersed in an irrotational fluid. We derive the equations governing the motion of the solid bodies *without explicitly incorporating the ambient fluid*. We then realize the equations in a convenient form for studying the *net locomotion of the solids as a function of the shape changes*. These goals are achieved by making use of the ideas of geometric mechanics—specifically, through the use of reduction, connections, and holonomy.

Problem Setting. Consider N solid bodies immersed in a (possibly infinitely large) volume of an incompressible fluid which is at rest at infinity. Assume that at any time t, the system consisting of the solid bodies and the fluid occupies a nonempty, open, connected region M of the two- or three-dimensional Euclidean space, which we identify with $\mathbb{R}^2$ or $\mathbb{R}^3$. For simplicity, assume that $M = \mathbb{R}^2$ or that $M = \mathbb{R}^3$. Further, let the solid bodies occupy regions $\mathcal{B}_i$, $i = 1, 2, \ldots, N$ and let the fluid occupy a connected region $\mathcal{F} \subset M$, so that M can be written as a disjoint union (apart from the common boundaries) as

$$M = \mathcal{B}_1 \cup \cdots \cup \mathcal{B}_N \cup \mathcal{F}.$$

As mentioned, we shall be using mainly techniques of geometric mechanics together with numerical simulations to solve the problem. These techniques have been useful in a number of other locomotion problems—mainly as a way to separate the shape variables from the overall locomotion variables. At the beginning, to make the exposition as accessible as we can, we limit our discussion to the configuration spaces and symmetry considerations, using language that is as familiar as possible. The key dynamical equations are written out at the beginning of Section 5 in classical language, but then one has to perform a reconstruction to get the actual movement of the system. As in rigid body mechanics, knowing Euler's equations is just a first step; to get the actual rotational motion of the body, one has to do a reconstruction to get the motion on the rotation group. Keep in mind that it is well known that using classical Euler angles for such a problem is generally not useful from a numerical point of view.

2.1. The Configuration Space

The configuration space Q for the system consisting of the solid bodies plus the fluid is the set of all (appropriately smooth) maps q from M to M with the following properties:

1. $q|_\infty$ is the identity.
2. $q|_\mathcal{F}$ represents the position field of the fluid particles and is volume-preserving. That is, $q|_\mathcal{F} \in \mathrm{Diff}_{\mathrm{vol}}(\mathcal{F})$, the set of volume-preserving diffeomorphisms of $\mathcal{F}$ that are the identity at infinity.
3. $q|_{\mathcal{B}_i}$, $i = 1, 2, \ldots, N$, represents the motion of the i^{th} solid body $\mathcal{B}_i \subset M$ with boundary $\partial\mathcal{B}_i$. For an elastic body (and in the absence of collisions, which we tacitly assume here), $q|_{\mathcal{B}_i}$ is normally taken to be an embedding of $\mathcal{B}_i$ in M (see Coutand and Shkoller [2004]). In the present work, we consider that $\mathcal{B}_i$ undergo rigid motions, that is, $q|_{\mathcal{B}_i}$ is an isometry and can be represented by $(R_i, \mathbf{r}_i)$, an element of the rigid body group SE(3). Here, $R_i \in \mathrm{SO}(3)$ is a rotation matrix that describes the orientation of $\mathcal{B}_i$, and $\mathbf{r}_i \in \mathbb{R}^3$ describes its position relative to a fixed inertial frame. For notational convenience, we will denote SE(3) by G and use $g_i = (R_i, \mathbf{r}_i) \in G$. Also, we denote the space of configurations of the submerged solids by $\mathcal{R}$, which can be defined naturally as
$$\mathcal{R} \subseteq \underbrace{\mathrm{SE}(3) \times \ldots \times \mathrm{SE}(3)}_{N \text{ times}}.$$
The subset $\mathcal{R}$ is defined in view of the constraints imposed on the bodies when they are connected via ball-and-socket or hinge joints, an issue that is discussed in Section 4.
4. We require that the union of the sets $q(\partial\mathcal{B}_i)$ (approached from the interior of $\mathcal{B}_i$) agrees with the set $q(\partial\mathcal{F})$ (approached from the interior of the fluid region $\mathcal{F}$) as sets, but we do not require that $q|_{\partial\mathcal{B}_i} = q|_{\partial\mathcal{F}}$ as maps; that is, the fluid may slip along the boundaries of the solid bodies.

2.2. Reduction by the Fluid Symmetry

We assume that the motion of the submerged solids sets the surrounding fluid into motion *without generating circulation*. In particular, if the fluid is irrotational in the reference configuration, it will remain irrotational at all times; that is, the notion of potential flow is well-defined. In this case, following Kirchhoff's theory for a solid moving in potential flow (see Lamb [1932]), we show that the dynamics of the solid-fluid system can be described in terms of solid variables only. In other words, the dynamics can be described on the phase space $T\mathcal{R}$ of the submerged solids parameterized by g_i and $\dot{g}_i$, $i = 1, \ldots, N$, only. In the geometric approach to fluid mechanics, the latter statement follows naturally from performing reduction at zero vorticity. The reduction procedure will be an important tool in generalizing the current study to include interactions with vortical flows (as in, for example, Shashikanth, Marsden, Burdick, and Kelly [2002] and Borisov and Mamaev [2003] and references therein) which, of course, play a crucial role in aquatic locomotion and will be addressed in future works. A brief discussion of the reduction procedure at zero vorticity is outlined below; the uninterested reader may skip directly to the next section.

Geometric Fluid Mechanics. There is a natural *right action* of $\mathrm{Diff}_{\mathrm{vol}}(\mathcal{F})$ on Q that is given by the composition on the right—that is, the action of $\eta \in \mathrm{Diff}_{\mathrm{vol}}(\mathcal{F})$ on $q \in Q$ is

$q \circ \eta$, where η is extended from $\mathcal{F}$ to M to be the identity mapping on $\mathcal{B}_1 \cup \cdots \cup \mathcal{B}_N$. Physically, this action of the group $\mathrm{Diff}_{\mathrm{vol}}(\mathcal{F})$ corresponds to a *relabeling of the fluid particles*.

It is well known in the geometric approach to fluid mechanics (see Arnold [1966], Ebin and Marsden [1969]) that the Lie algebra of $\mathrm{Diff}_{\mathrm{vol}}(\mathcal{F})$ consists of the space of volume-preserving vector fields $\mathfrak{X}_{\mathrm{div}}(\mathcal{F})$ (with the Lie bracket being the Jacobi-Lie bracket of vector fields), and its dual may be regarded as the space of vorticity fields, as is explained in Marsden and Weinstein [1983]. Further, the momentum map $J_{\mathcal{F}} : T^*Q \to \mathfrak{X}^*_{\mathrm{div}}(\mathcal{F})$ associated with the action of $\mathrm{Diff}_{\mathrm{vol}}(\mathcal{F})$ on Q and hence on T^*Q is given by vorticity advection (see, for example, Marsden and Weinstein [1983] and Marsden, Pekarsky, Shkoller, and West [2001]). Any reasonable fluid Lagrangian will be $\mathrm{Diff}_{\mathrm{vol}}(\mathcal{F})$-invariant (corresponding to the fact that all the fluid particles are identical, known as *particle-relabeling symmetry*) and so will give equations of motion that preserve circulation.

Hamiltonian Reduction. For potential flow where $J_{\mathcal{F}} = 0$, we can carry out symplectic reduction at zero to get, as the reduced space,

$$J_{\mathcal{F}}^{-1}(0)/\mathrm{Diff}_{\mathrm{vol}}(\mathcal{F}) \;=\; T^*(Q/\mathrm{Diff}_{\mathrm{vol}}(\mathcal{F})) = T^*\mathcal{R}, \tag{2.1}$$

where $Q/\mathrm{Diff}_{\mathrm{vol}}(\mathcal{F})$ is identified with $\mathcal{R}$ as the set of maps that take the solid bodies from their reference to current configuration. In obtaining equation (2.1), we have evoked the well-known fact (see, for example, Marsden [1992]) that reduction of T^*Q by a group G at the zero level of the momentum map is just the cotangent bundle of shape space: $T^*(Q/G)$ with its standard canonical symplectic structure. An initial Hamiltonian $H : T^*Q \to \mathbb{R}$ that is invariant under G naturally induces a Hamiltonian on $T^*(Q/G)$, and the dynamics also naturally drops from T^*Q to $T^*(Q/G)$.

Lagrangian Reduction. Similarly, if one is dealing with Lagrangian mechanics, starting with a Lagrangian $L_Q : TQ \to \mathbb{R}$, then one can make use of Routh reduction at zero (see, for example, Marsden and Scheurle [1993] and Marsden, Ratiu, and Scheurle [2000]), and one ends up with a reduced Lagrangian (which at the momentum value zero coincides with the Routhian) on the tangent bundle of shape space, $T(Q/G)$—that is, $T\mathcal{R}$ in our case. For convenience, we shall be working mainly in the context of Lagrangian mechanics in this paper.

3. The Lagrangian Function

For a system of solid bodies submerged in an incompressible fluid with no external forces and torques, the Lagrangian function L_Q is equal to the total kinetic energy of the system, that is, the kinetic energy of the fluid $T_{\mathcal{F}}$ plus the energies of the solid bodies $T_{\mathcal{B}_i}$; namely,

$$L_Q = T_{\mathcal{F}} + \sum_{i=1}^{N} T_{\mathcal{B}_i}. \tag{3.1}$$

The kinetic energy of the fluid $T_{\mathcal{F}}$ is given in spatial representation by

$$T_{\mathcal{F}} = \frac{1}{2}\int_{\mathcal{F}} \rho_{\mathcal{F}} |\mathbf{u}|^2 \, \mathrm{d}v, \tag{3.2}$$

where $\rho_{\mathcal{F}}$ is the mass density of the fluid, $\mathbf{u}$ is its spatial velocity field, and $\mathrm{d}v$ is the standard volume element on $\mathbb{R}^3$.

Recall that the submerged solids undergo rigid motions described by $g_i = (R_i, \mathbf{r}_i)$, where R_i are the rotation matrices and $\mathbf{r}_i$ denote the position vectors of $\mathcal{B}_i$. Let $\mathbf{\Omega}_i$ and $\mathbf{v}_i$ be, respectively, the angular and translational velocity vectors of the i^{th} body represented relative to the $\mathcal{B}_i$-fixed frame. One can readily verify that

$$\hat{\mathbf{\Omega}}_i = R_i^{-1}\dot{R}_i, \qquad \mathbf{v}_i = R_i^{-1}\dot{\mathbf{r}}_i, \tag{3.3}$$

where the symbol $\hat{()}$ refers to the map $\hat{}\colon \mathbb{R}^3 \to \mathfrak{so}(3)$ given by[3] $\hat{\boldsymbol{\alpha}}\boldsymbol{\beta} = \boldsymbol{\alpha} \times \boldsymbol{\beta}$ for all $\boldsymbol{\alpha}, \boldsymbol{\beta} \in \mathbb{R}^3$. The kinetic energy $T_{\mathcal{B}_i}$ can then be written as

$$T_{\mathcal{B}_i} = \frac{1}{2}\Big(\mathbf{\Omega}_i \cdot \mathcal{I}_i \mathbf{\Omega}_i + \mathbf{v}_i \cdot m_i \mathbf{v}_i\Big), \tag{3.4}$$

where $\mathcal{I}_i$ is the second-order moment of inertia tensor of $\mathcal{B}_i$, and m_i its mass. Here, we emphasize that the submerged bodies are neutrally buoyant and that the body-fixed frames are placed at the respective mass centers.

3.1. Rewriting the Kinetic Energy of the Fluid

The main goal of this section is to follow the classical procedure of Kirchhoff (see Lamb [1932]) to obtain from $L_Q : TQ \to \mathbb{R}$ a reduced Lagrangian $L_{\mathcal{R}} : T\mathcal{R} \to \mathbb{R}$, by deriving an expression for $T_{\mathcal{F}}$ as a function of only the variables associated with the solid bodies.

Recall that the region $\mathcal{F}$ is connected; hence, if the flow is irrotational and has zero circulation, we can write the velocity field in terms of a potential ϕ, i.e.,

$$\mathbf{u} = \nabla\phi. \tag{3.5}$$

Incompressibility of course implies that the Laplacian of ϕ is zero,

$$\triangle\, \phi = 0. \tag{3.6}$$

Now, substitute (3.5) into (3.2) and use the identity

$$\mathrm{div}(\phi\nabla\phi) = \nabla\phi \cdot \nabla\phi + \phi \,\triangle\, \phi,$$

together with (3.6). Then, invoke Green's theorem, taking into consideration that the fluid is at rest at infinity, to get

$$T_{\mathcal{F}} = -\frac{1}{2}\int_{\sum_{i=1}^{N} \partial\mathcal{B}_i} \phi\nabla\phi \cdot \mathbf{n} \, \mathrm{d}a, \tag{3.7}$$

[3] Here, $\mathfrak{so}(3)$ is the space of 3×3 skew-symmetric matrices, the Lie algebra of the Lie group of rigid-body rotations SO(3).

where the integration reduces to an integration over the boundaries of the solid bodies $\partial\mathcal{B}_i$, $\mathbf{n}$ is the outward (into the fluid) normal vector to $\partial\mathcal{B}_i$, and $\mathrm{d}a$ is an infinitesimal area element of $\partial\mathcal{B}_i$.

The potential ϕ may be expressed as a function of the configurations and velocities of the submerged bodies (Lamb [1932]). To prove this statement, we write the potential ϕ in the Kirchhoff form, as follows:

$$\phi = \sum_{i=1}^{N} \left(\boldsymbol{\Omega}_i \cdot \boldsymbol{\chi}_i + \mathbf{v}_i \cdot \boldsymbol{\varphi}_i \right), \tag{3.8}$$

where the components of $\boldsymbol{\varphi}_i$ represent translational velocity potentials associated with the i^{th} body and the components of $\boldsymbol{\chi}_i$ are rotational velocity potentials. Clearly, $\boldsymbol{\varphi}_i$ and $\boldsymbol{\chi}_i$ are dimensionally inhomogeneous; they have units of length and length squared, respectively.

From Property 4 of the map q defined in Section 2, one has that the normal velocity of the fluid, given by $\nabla\phi \cdot \mathbf{n}$ $(= \partial\phi/\partial n)$ at any point of $\partial\mathcal{B}_i$, is equal to the normal velocity of the surface $\partial\mathcal{B}_i$ at that point, that is,

$$\left.\frac{\partial \phi}{\partial n}\right|_{\partial\mathcal{B}_i} = (\Omega_i \times \mathbf{X}_i + \mathbf{v}_i) \cdot \mathbf{n}_i, \tag{3.9}$$

where $\mathbf{n}_i$ denotes the normal vector to $\partial\mathcal{B}_i$ and $\mathbf{X}_i$ is the position vector to a given material point of $\mathcal{B}_i$, in particular, of $\partial\mathcal{B}_i$. By virtue of (3.8) and (3.9), one gets

$$\frac{\partial \boldsymbol{\chi}_i}{\partial n} = \mathbf{X}_i \times \mathbf{n}_i, \qquad \frac{\partial \boldsymbol{\varphi}_i}{\partial n} = \mathbf{n}_i. \tag{3.10}$$

Hence, $\boldsymbol{\varphi}_i$ and $\boldsymbol{\chi}_i$ depend on only the geometry of the submerged rigid bodies and are simply solutions of Laplace's equation with the Neumann boundary conditions (3.10); see Section 7.2 for further details.

To obtain an expression for the kinetic energy of the fluid in terms of the geometry and velocities of the submerged bodies, one needs to substitute (3.8) back into (3.7). To this end, it can readily be verified that

$$T_{\mathcal{F}} = \frac{1}{2} \sum_{i=1}^{N} \sum_{j=1}^{N} \left(\boldsymbol{\Omega}_i \cdot \Theta_{ij}^{\chi\chi} \boldsymbol{\Omega}_j + \boldsymbol{\Omega}_i \cdot \Theta_{ij}^{\chi\varphi} \mathbf{v}_j + \mathbf{v}_i \cdot \Theta_{ij}^{\varphi\chi} \boldsymbol{\Omega}_j + \mathbf{v}_i \cdot \Theta_{ij}^{\varphi\varphi} \mathbf{v}_j \right), \tag{3.11}$$

where $\Theta_{ij}^{\chi\chi}$ and $\Theta_{ij}^{\varphi\varphi}$ are of the form[4]

$$\Theta_{ij}^{\chi\chi} = \rho_{\mathcal{F}} \int_{\partial\mathcal{B}_j} \boldsymbol{\chi}_i \otimes \frac{\partial \boldsymbol{\chi}_j}{\partial n}\, \mathrm{d}a, \qquad \Theta_{ij}^{\varphi\varphi} = \rho_{\mathcal{F}} \int_{\partial\mathcal{B}_j} \boldsymbol{\varphi}_i \otimes \frac{\partial \boldsymbol{\varphi}_j}{\partial n}\, \mathrm{d}a, \tag{3.12}$$

while $\Theta_{ij}^{\chi\varphi}$ and $\Theta_{ij}^{\varphi\chi}$ are given by

$$\Theta_{ij}^{\chi\varphi} = \frac{1}{2}\, \rho_{\mathcal{F}} \left(\int_{\partial\mathcal{B}_j} \boldsymbol{\chi}_i \otimes \frac{\partial \boldsymbol{\varphi}_j}{\partial n} \mathrm{d}a + \int_{\partial\mathcal{B}_i} \frac{\partial \boldsymbol{\chi}_i}{\partial n} \otimes \boldsymbol{\varphi}_j\, \mathrm{d}a \right), \tag{3.13}$$

[4] The tensor associated with the product $\mathbf{a} \otimes \mathbf{b}$ is defined through its operation on $\mathbf{c}$: $(\mathbf{a} \otimes \mathbf{b})\mathbf{c} = (\mathbf{b} \cdot \mathbf{c})\mathbf{a}$.

and

$$\Theta_{ij}^{\varphi\chi} = \frac{1}{2}\,\rho_{\mathcal{F}} \left(\int_{\partial \mathcal{B}_j} \boldsymbol{\varphi}_i \otimes \frac{\partial \boldsymbol{\chi}_j}{\partial n} \mathrm{d}a + \int_{\partial \mathcal{B}_i} \frac{\partial \boldsymbol{\varphi}_i}{\partial n} \otimes \boldsymbol{\chi}_j \,\mathrm{d}a \right). \tag{3.14}$$

Remark. It should be clear from writing (3.8) that we regard the velocity potentials $\boldsymbol{\chi}_i$ and $\boldsymbol{\varphi}_i$ as written relative to the $\mathcal{B}_i$-fixed frame. This means, by virtue of (3.12)–(3.14), that $\Theta_{ii}^{\chi\chi}, \ldots, \Theta_{ii}^{\varphi\chi}$ are expressed in the i^{th}-frame, while $\Theta_{ij}^{\chi\chi}, \ldots, \Theta_{ij}^{\varphi\chi}$ are two-point matrices with one leg in the i^{th}-frame and the second leg in the j^{th}-frame.

The Added Inertias. The values in (3.12)–(3.14) are called "added inertias" and can be written in the convenient 6×6 matrix form

$$\mathbb{M}_{ij}^{f} = \begin{pmatrix} \Theta_{ij}^{\chi\chi} & \Theta_{ij}^{\chi\varphi} \\ \Theta_{ij}^{\varphi\chi} & \Theta_{ij}^{\varphi\varphi} \end{pmatrix}, \tag{3.15}$$

where $\mathbb{M}_{ij}^{f}$ are functions of $\rho_{\mathcal{F}}$ and the configurations g_i of the submerged bodies, as discussed above.

Symmetry Properties. The added inertia matrices $\mathbb{M}_{ij}^{f}$ have two symmetry properties; namely,

$$(\mathbb{M}_{ij}^{f})^T = \mathbb{M}_{ij}^{f}, \tag{3.16}$$

and

$$\mathbb{M}_{ji}^{f} = \mathbb{M}_{ij}^{f}. \tag{3.17}$$

To confirm (3.16), consider two potential functions φ^1 and φ^2 in the fluid domain $\mathcal{F}$ (i.e., solutions of Laplace's equation); more specifically, let φ^1 and φ^2 be distinct components of $\boldsymbol{\varphi}_1$. Then, apply the divergence theorem to the following integral quantity to get

$$\int_{\sum_i^N \partial \mathcal{B}_i} \left(\varphi^1 \frac{\partial \varphi^2}{\partial n} - \varphi^2 \frac{\partial \varphi^1}{\partial n} \right) \mathrm{d}a = - \int_{\mathcal{F}} \nabla \left(\varphi^1 \nabla \varphi^2 - \varphi^2 \nabla \varphi^1 \right) \mathrm{d}v = 0.$$

By virtue of the above identity and definition $(3.12)_2$, one can readily conclude that $\Theta_{11}^{\varphi_1\varphi_2} = \Theta_{11}^{\varphi_2\varphi_1}$. A similar argument holds for the remaining components; in particular, one has $\Theta_{ij}^{\chi\varphi} = \Theta_{ij}^{\varphi\chi}$.

The symmetry in (3.17) can easily be seen by renaming indices of the right-hand side of (3.11) and using the previous symmetry. For example, consider $\boldsymbol{\Omega}_i \cdot \Theta_{ij}^{\chi\chi} \boldsymbol{\Omega}_j$ and write

$$\boldsymbol{\Omega}_i \cdot \Theta_{ij}^{\chi\chi} \boldsymbol{\Omega}_j \;=\; \boldsymbol{\Omega}_j \cdot \Theta_{ji}^{\chi\chi} \boldsymbol{\Omega}_i \;=\; \boldsymbol{\Omega}_i \cdot \left(\Theta_{ji}^{\chi\chi} \right)^T \boldsymbol{\Omega}_j = \boldsymbol{\Omega}_i \cdot \Theta_{ji}^{\chi\chi} \boldsymbol{\Omega}_j, \tag{3.18}$$

which yields $\Theta_{ij}^{\chi\chi} = \Theta_{ji}^{\chi\chi}$. The same holds for $\Theta_{ij}^{\varphi\varphi}$ and $\Theta_{ij}^{\chi\varphi}$, and hence, $\mathbb{M}_{ij}^{f} = \mathbb{M}_{ji}^{f}$. This symmetry reflects a reciprocity in the effects any two submerged bodies i and j have on each other.

3.2. The Reduced Lagrangian

Let ξ_i represent the angular and translational velocities of $\mathcal{B}_i$ with respect to $\mathcal{B}_i$-fixed frame; namely, write

$$\xi_i = \begin{pmatrix} \boldsymbol{\Omega}_i \\ \mathbf{v}_i \end{pmatrix}. \tag{3.19}$$

This notation is consistent with the group theoretic notation $\xi_i = g_i^{-1}\dot{g}_i$—see Appendix A—and will be used in the remainder of this paper for conciseness. Correspondingly, we rewrite the actual mass and moments of inertia of $\mathcal{B}_i$ in the form

$$\mathbb{M}_i^b = \begin{pmatrix} \mathcal{I}_i & 0 \\ 0 & m_i\mathbf{I} \end{pmatrix}, \tag{3.20}$$

where $\mathbf{I}$ is the 3×3 identity matrix. By virtue of (3.19)–(3.20) and (3.15), the kinetic energy of the solids (3.4) and that of the fluid (3.11) can be expressed, respectively, as

$$T_b = \sum_i \frac{1}{2}\,\xi_i^T \mathbb{M}_i^b \xi_i, \quad \text{and} \quad T_f = \sum_i \sum_j \frac{1}{2}\,\xi_i^T \mathbb{M}_{ij}^f \xi_j. \tag{3.21}$$

Now, substitute (3.21) back into (3.1) in order to obtain the following expression for the reduced Lagrangian as a function of g_i and ξ_i only:

$$L_R(g_i, \xi_i) = \frac{1}{2}\sum_{i=1}^{3}\sum_{j=1}^{3} \xi_i^T\, \mathbb{I}_{ij}\, \xi_j, \tag{3.22}$$

where $\mathbb{I}_{ij} = \mathbb{M}_{ij}^f$ for $i \neq j$ and $\mathbb{I}_{ii} = \mathbb{M}_i^b + \mathbb{M}_{ii}^f$ for $i = j$. Note that, although there is an analogy between $\mathbb{M}_{ij}^f$ and $\mathbb{M}_i^b$, they are fundamentally distinct. For example, in translation, unlike the body's actual mass, the added inertia $\mathbb{M}_{ij}^f$ may differ depending on the direction of the body's motion.

Invariance of $L_{\mathcal{R}}$ under Superimposed Rigid Motions. The Lagrangian function in (3.22) is invariant under superimposed rigid motions. This can readily be seen by noting that the added inertias $\mathbb{M}_{ij}^f$ depend, by definition, on the *shape*, that is, the relative configurations of the submerged bodies, and are not affected by the choice of inertial frame. The invariance corresponds to a symmetry in the dynamics on $T\mathcal{R}$, namely, the conservation of the total momentum of the solid-fluid system, and can be exploited to obtain reduced equations of motion, as discussed in Section 5. But, beforehand, we examine the structure of the configuration space $\mathcal{R}$.

4. Structure of the Configuration Space

In Section 2.1, the configuration space $\mathcal{R}$ of N submerged rigid bodies was naturally chosen to be the direct product group

$$\mathcal{R} = \underbrace{G \times \cdots \times G}_{N \text{ times}},$$

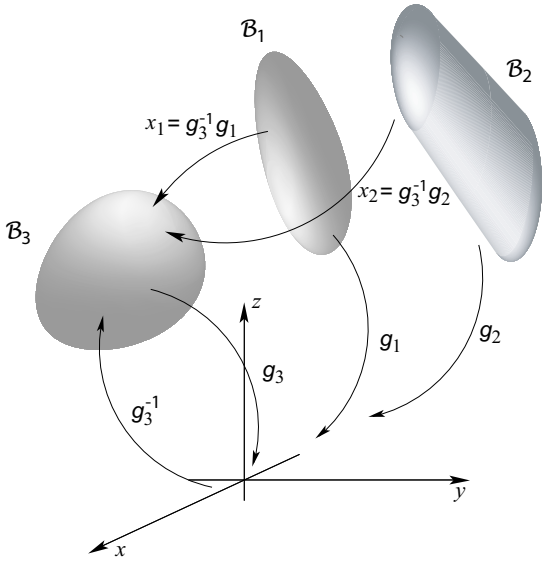

Fig. 2. The rigid motions of $\mathcal{B}_i$, $i = 1, 2, 3$, relative to a fixed inertial frame, are given by g_i, respectively, while the rigid motions of $\mathcal{B}_\alpha$, $\alpha = 1, 2$, relative to a $\mathcal{B}_3$-fixed frame, are given by $g_3^{-1} g_\alpha$.

where G denotes the group of rigid motions $G = \mathrm{SE}(3)$. For concreteness, consider $N = 3$, and let $x_1 = g_3^{-1} g_1$ and $x_2 = g_3^{-1} g_2$ denote the rigid motions of $\mathcal{B}_1$ and $\mathcal{B}_2$ relative to $\mathcal{B}_3$ as shown in Figure 2.

Constraints. We connect the bodies, say via ball-and-socket or hinge joints, in order to obtain a system of articulated rigid bodies. In the articulated system, two linked bodies can rotate freely relative to each other, but their relative positions are constrained. In other words, the degrees of freedom in the *relative* motions (x_1, x_2) correspond purely to rotational variables. For a comprehensive discussion of the dynamics of planar rigid bodies coupled via hinge joints, the reader is referred to Sreenath, Oh, Krishnaprasad, and Marsden [1988] and Oh, Sreenath, Krishnaprasad, and Marsden [1989].

The Shape Space. We refer to the space of admissible relative motions (x_1, x_2) as the shape space $\mathfrak{X}$. Clearly, (x_1, x_2) completely determine the shape of the three-body system but not its position and orientation relative to a fixed inertial frame. The latter information is given by g_3; hence, the configuration of the solids can be described fully using (x_1, x_2, g_3). That is, $\mathcal{R}$ can be identified with the space $\mathcal{R} \equiv \mathfrak{X} \times G$.

The Bundle Structure. One can show that the configuration space $\mathcal{R}$ forms a principal bundle over the shape space $\mathfrak{X}$ whose fibers are G; see Appendix B. That is, roughly speaking, at each point (x_1, x_2) of the shape space, one has a copy of the group of rigid motions; see Figure 3.

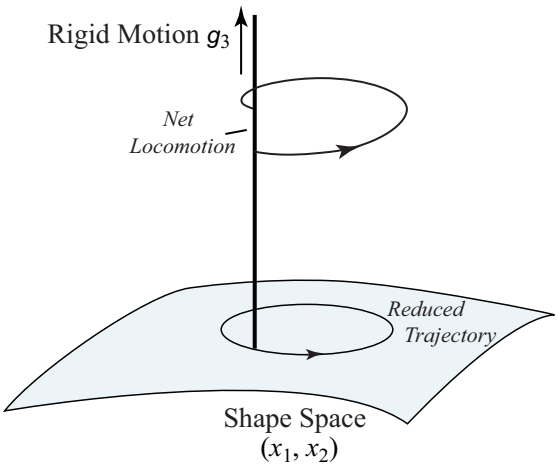

Fig. 3. The configuration space $\mathcal{R}$ has the structure of a principal bundle over the shape space $\mathfrak{X}$, which allows the net locomotion g_3 to be cast as a geometric phase, or holonomy, over closed loops traced by the shape variables (x_1, x_2).

This geometric picture is very convenient to address the locomotion problem—namely, whether a net rigid motion can be achieved as a result of (x_1, x_2) tracing a *closed* loop in the shape space. In order to investigate this issue, we first need to derive the equations governing the dynamic coupling between the shape variables and the group motion.

5. The Equations of Motion

As mentioned before, the Lagrangian in (3.22) is invariant under rigid motions superimposed on the solid-fluid system.[5] This invariance corresponds to a symmetry in the dynamics on $T\mathcal{R}$, namely, the conservation of the total momentum of the solid-fluid system.

It is well known in mechanics that the presence of conserved quantities can be exploited to eliminate some of the variables and to reduce the number of equations needed to describe the dynamics. In this section, we use Lagrangian reduction (see Cendra, Marsden, and Ratiu [2001]) in order to eliminate the g_3 variables and describe the dynamics in terms of $(x_1, x_2, \xi_1, \xi_2, \xi_3)$ only. We first summarize the resulting equations; the uninterested reader may skip the details of the derivation.

[5] This is not to be confused with rigid motions superimposed on the submerged bodies alone. Clearly, such motion does not conserve L_R, in general.

We associate with each submerged body $\mathcal{B}_i$ a *momentum-like* quantity h_i expressed relative to $\mathcal{B}_i$-fixed frame as follows:

$$h_i = \sum_{j=1}^{3} \mathbb{I}_{ij} \xi_j. \tag{5.1}$$

The total momentum of the system of solids and fluid expressed relative to the $\mathcal{B}_3$-fixed frame can then be written as

$$h_s = \widetilde{h_1} + \widetilde{h_2} + h_3, \tag{5.2}$$

where $\widetilde{h_1}$ and $\widetilde{h_2}$ correspond to h_1 and h_2 when transformed from their respective body-fixed frames to the $\mathcal{B}_3$-fixed frame. It is important to note, however, that one cannot assert that h_s is the total momentum of the system, which in this problem is indeterminate (since the fluid has an infinite domain). Traditionally, h_s was known as the "impulse" (see Lamb [1932, Chapter 6]). $\mathbf{\Pi}$

The momenta h_i can be rewritten as $h_i = (\mathbf{\Pi}_i, \mathbf{P}_i)^T$, where $\mathbf{\Pi}_i$ and $\mathbf{P}_i$ denote, respectively, the *body* angular and linear momenta vectors. Similarly, we introduce $h_s = (\mathbf{\Pi}_s, \mathbf{P}_s)^T$. The governing equations of motion are given by

$$\begin{aligned} \dot{\mathbf{\Pi}}_s &= \mathbf{\Pi}_s \times \mathbf{\Omega}_3 + \mathbf{P}_s \times \mathbf{v}_3, \\ \dot{\mathbf{P}}_s &= \mathbf{P}_s \times \mathbf{\Omega}_3, \end{aligned} \tag{5.3}$$

together with

$$\begin{aligned} \dot{\mathbf{\Pi}}_1 &= \mathbf{\Pi}_1 \times \mathbf{\Omega}_1 + \mathbf{P}_1 \times \mathbf{v}_1 + \boldsymbol{\tau}_1, \\ \dot{\mathbf{\Pi}}_2 &= \mathbf{\Pi}_2 \times \mathbf{\Omega}_2 + \mathbf{P}_2 \times \mathbf{v}_2 + \boldsymbol{\tau}_2, \end{aligned} \tag{5.4}$$

where $\boldsymbol{\tau}_1$ and $\boldsymbol{\tau}_2$ denote the torques applied at the joints. Recall that the degrees of freedom in (x_1, x_2) correspond to relative rotations, and hence, in (5.4), we needed to write only the equations governing the angular motion. Finally, it is worth noting that (5.3) have the same form as Kirchhoff's equations of motion for one rigid body in an ideal fluid, which were derived in Leonard [1997] using Lie-Poisson reduction.

5.1. The Reduced Phase Space

In this section, we rewrite the Lagrangrian L_R as a reduced Lagrangian function on a properly defined phase space $\mathfrak{R}$ and discuss the geometry of variations on this space.

Relative Velocities. We remind the reader that ξ_i, defined in (3.19), denote the angular and linear velocities of $\mathcal{B}_i$ expressed with respect to $\mathcal{B}_i$-fixed frame. Now, define ζ_α, $\alpha = 1, 2$, to be the velocities of $\mathcal{B}_\alpha$ relative to $\mathcal{B}_3$ but expressed with respect to $\mathcal{B}_\alpha$-fixed frames. The velocities ξ_α can then be rewritten in the form

$$\xi_\alpha = \zeta_\alpha + \mathrm{Ad}_{x_\alpha^{-1}} \xi_3, \tag{5.5}$$

where $\mathrm{Ad}_{x_\alpha^{-1}}$ denote the operators (6×6 matrices) that transform ξ_3 from $\mathcal{B}_3$-fixed frame to the respective $\mathcal{B}_\alpha$-fixed frame; see Appendix A.

The Reduced Lagrangian l. Recall that, when expressed in the body-fixed frames, the added inertias $\mathbb{M}_{ij}^f$ depend only on the relative configurations of the submerged bodies, that is, $\mathbb{M}_{ij}^f = \mathbb{M}_{ij}^f(x_1, x_2)$ only. Hence, L_R in (3.22) can be thought of as a function of $(x_1, x_2, \xi_1, \xi_2, \xi_3)$, rather than as a function on $T\mathcal{R}$. Now, by virtue of (5.5), one can identify any function of $(x_1, x_2, \xi_1, \xi_2, \xi_3)$ with a function of $(x_1, x_2, \zeta_1, \zeta_2, \xi_3)$. In particular, $L_R(x_1, x_2, \xi_1, \xi_2, \xi_3)$ is identified with $l(x_1, x_2, \zeta_1, \zeta_2, \xi_3)$ on the *reduced* phase space $\mathfrak{R}$ parameterized by $(x_1, x_2, \zeta_1, \zeta_2, \xi_3)$. This result is due to the principal bundle structure of $\mathcal{R}$ and the presence of the connection A on $T\mathcal{R}$ and is formally proven in Appendix B following the work of Cendra, Marsden, and Ratiu [2001].

Vertical and Horizontal Directions. The phase space $\mathfrak{R}$ parameterized by $(x_1, x_2, \zeta_1, \zeta_2, \xi_3)$ can naturally be split into *vertical* and *horizontal* directions spanned by

$$d^{\mathrm{v}} = (0, 0, 0, 0, \xi_3), \quad \text{and} \quad d^h = (x_1, x_2, \zeta_1, \zeta_2, 0).$$

This can readily be verified by noting that ξ_3 and $(x_1, x_2, \zeta_1, \zeta_2)$ are *independent variables* by definition. It is important to point out that the use of the words *vertical* and *horizontal* may be thought of as merely a notation to distinguish the two directions. In essence, this notation is chosen for its consistency with the development in Appendix B.

Vertical Variations. A variation δg_3 on the rigid motion g_3 induces a *vertical* variation $\delta\xi_3$ on the associated velocity $\xi_3 = g_3^{-1}\dot{g}_3$. The variation $\delta\xi_3$ is constrained to be of the form

$$\delta\xi_3 = \dot{\eta}_3 + \mathrm{ad}_{\xi_3}\,\eta_3, \tag{5.6}$$

where $\eta_3 = g_3^{-1}\delta g_3$ and the operator ad_{ξ_3} is defined in (A.6). For a proof of (5.6), see Appendix B. From (5.5), one can readily conclude that a vertical variation $\delta\xi_3$ induces vertical variations $\delta^{\mathrm{v}}\xi_\alpha$ on ξ_α of the form

$$\delta^{\mathrm{v}}\xi_\alpha = \mathrm{Ad}_{x_\alpha^{-1}}\,\delta\xi_3. \tag{5.7}$$

Horizontal Variations. Analogously, variations δx_α on the relative rigid motion x_α induce variations $\delta\zeta_\alpha$ on the associated relative velocities $\zeta_\alpha = x_\alpha^{-1}\dot{x}_\alpha$ of the form

$$\delta\zeta_\alpha = \dot{\gamma}_\alpha + \mathrm{ad}_{\zeta_\alpha}\,\gamma_\alpha, \tag{5.8}$$

where $\gamma_\alpha = x_\alpha^{-1}\delta x_\alpha$. Clearly, $(\delta x_1, \delta x_2, \delta\zeta_1, \delta\zeta_2)$ are horizontal variations, and they induce *horizontal* variations on $\xi_\alpha, \alpha = 1, 2$, but not on ξ_3. Indeed, due to the dependence of g_α on x_α, δx_α induce variations δg_α which, in turn, give rise to horizontal variations $\delta^h\xi_\alpha$ on the associated velocities $\xi_\alpha = g_\alpha^{-1}\dot{g}_\alpha$. The variations $\delta^h\xi_\alpha$ must be of the form

$$\delta^{\mathrm{h}}\xi_\alpha = \dot{\eta}_\alpha + \mathrm{ad}_{\xi_\alpha}\,\eta_\alpha, \tag{5.9}$$

where $\eta_\alpha = g_\alpha^{-1}\delta g_\alpha$. Finally, note that δx_α does not affect ξ_3 since x_α and g_3 are independent variables.

5.2. The Lagrange-Poincaré Equations

As argued before, the Lagrangian function in (3.22) is rewritten, by virtue of (5.5), as

$$l(x_1, x_2, \zeta_1, \zeta_2, \xi_3) = \frac{1}{2}\xi_i^T \mathbb{I}_{ij}\xi_j, \tag{5.10}$$

where summation is implied on repeated indices. The associated Lagrange-Poincaré equations are derived using the reduced variational principle which, by virtue of (5.1), takes the form

$$\delta \int_{t_0}^{t_f} l(x_1, x_2, \zeta_1, \zeta_2, \xi_3)\, \mathrm{d}t = \int_{t_0}^{t_f} h_i^T\, \delta\xi_i\, \mathrm{d}t = 0. \tag{5.11}$$

The Vertical Lagrange-Poincaré Equations. These equations correspond to vertical variations. Hence, they are derived by first replacing $\delta\xi_\alpha$ in (5.11) by their values $\delta^{\mathrm{v}}\xi_\alpha$ from (5.7) in order to get

$$\int_{t_0}^{t_f} h_i^T\, \delta^{\mathrm{v}}\xi_i\, \mathrm{d}t = \int_{t_0}^{t_f} {h_s}^T\, \delta\xi_3\, \mathrm{d}t = 0. \tag{5.12}$$

Recall from (5.2) that h_s is the total momentum of the system

$$h_s = \mathrm{Ad}^T_{x_1^{-1}}(\mathbb{I}_{1j}\xi_j) + \mathrm{Ad}^T_{x_2^{-1}}(\mathbb{I}_{2j}\xi_j) + \mathbb{I}_{3j}\xi_j, \tag{5.13}$$

where $\mathrm{Ad}^T_{x_1^{-1}}$ and $\mathrm{Ad}^T_{x_2^{-1}}$ represent the operators that transform h_1 and h_2 from their respective body-fixed frames to the $\mathcal{B}_3$-fixed frame; see Appendix A. Now, substitute (5.6) into (5.12) to obtain, upon integrating by parts,

$$\int_{t_0}^{t_f} h_s\, \delta\xi_3\, \mathrm{d}t = \int_{t_0}^{t_f} -\dot{h}_s^T \eta_3 + h_s^T \mathrm{ad}_{\xi_3}\, \eta_3\, \mathrm{d}t = 0, \tag{5.14}$$

which is true for arbitrary η_3, and hence the vertical equations

$$\dot{h}_s = \mathrm{ad}^T_{\xi_3}\, h_s. \tag{5.15}$$

One can verify, upon introducing $h_s = (\mathbf{\Pi}_s, \mathbf{P}_s)^T$ and using (A.6), that (5.15) can be rewritten as

$$\begin{pmatrix} \dot{\mathbf{\Pi}}_s \\ \dot{\mathbf{P}}_s \end{pmatrix} = \begin{pmatrix} \hat{\mathbf{\Omega}}_3 & \hat{\mathbf{v}}_3 \\ 0 & \hat{\mathbf{\Omega}}_3 \end{pmatrix} \begin{pmatrix} \mathbf{\Pi}_s \\ \mathbf{P}_s \end{pmatrix}. \tag{5.16}$$

This, in turn, leads to (5.3).

Constant of Motion. Let H_s be the total momentum written relative to a fixed inertial frame. One has

$$H_s = \mathrm{Ad}^T_{g_3^{-1}} h_s, \tag{5.17}$$

where $\mathrm{Ad}^T_{g_3^{-1}}$ transforms h_s from the $\mathcal{B}_3$-fixed frame to the inertial frame. One can verify by taking the time derivative of (5.17) and invoking (5.15) that $\dot{H}_s = 0$, which confirms that H_s is indeed a constant of motion, as mentioned before.

Remark. Note that (5.15) are equivalent to Euler-Poincaré equations on the dual space $\mathfrak{R}^*$. This result—namely, the equivalence between the vertical Lagrange-Poincaré equations and the Euler-Poincaré—holds for an arbitrary Lie group G acting on a principal bundle $Q \to Q/G$ such that the Lagrangian L is left invariant. This statement can readily be proven following Theorem 13.5.3 of Marsden and Ratiu [1999].

The Horizontal Lagrange-Poincaré Equations. The horizontal Lagrange-Poincaré equations are derived following the same procedure while replacing $\delta\xi_\alpha$ in (5.11) by the respective horizontal variations $\delta^{\mathrm{h}}\xi_\alpha$ from (5.9). One gets

$$\dot{h}_\alpha = \mathrm{ad}^T_{\xi_\alpha} h_\alpha. \tag{5.18}$$

The Applied Torques. The submerged bodies are linked via joints equipped with motors that generate torques $\boldsymbol{\tau}_1$ and $\boldsymbol{\tau}_2$ to set bodies $\mathcal{B}_1$ and $\mathcal{B}_2$ in motion relative to $\mathcal{B}_3$. In this case, (5.11) has to be rewritten as the Lagrange-D'Alembert variational principle,

$$\delta \int_{t_0}^{t_f} l(x_1, x_2, \xi_1, \xi_2, \xi_3)\, \mathrm{d}t + \int_{t_0}^{t_f} \boldsymbol{\tau}_\alpha \cdot \delta R^{rel}_\alpha = 0, \tag{5.19}$$

where R^{rel}_α are relative rotations; remember that x_α can be written as $x_\alpha = (R^{rel}_\alpha, \mathbf{r}^{rel}_\alpha)$. Clearly, the additional term in (5.19) does not affect (5.15) but adds a torque vector to the right-hand side of (5.18). The properly modified horizontal equations lead to (5.4). We leave the details of this computation to the interested reader.

6. The Reconstruction Equations

Although the total momentum of the system H_s is conserved, its $\mathcal{B}_3$-fixed form h_s varies according to (5.3) or, equivalently, (5.15). In this section, we rewrite these equations in a form that is very convenient for studying locomotion.

When the motion starts from rest, h_s remains identically zero throughout the motion of the system; hence,

$$h_s = \mathrm{Ad}^T_{x_\alpha^{-1}}(\mathbb{I}_{\alpha j}\xi_j) + \mathbb{I}_{3j}\xi_j = 0, \tag{6.1}$$

where summation is implied on repeated indices. Substitute (5.5) into (6.1) and regroup terms to get

$$\mathbb{I}_{\mathrm{loc}}\,\xi_3 + \left(\mathrm{Ad}^T_{x_\alpha^{-1}}\mathbb{I}_{\alpha\beta} + \mathbb{I}_{3\beta}\right)\zeta_\beta = 0, \tag{6.2}$$

where

$$\mathbb{I}_{\mathrm{loc}} = \mathrm{Ad}^T_{x_\alpha^{-1}}\mathbb{I}_{\alpha\beta}\mathrm{Ad}_{x_\beta^{-1}} + \mathrm{Ad}^T_{x_\alpha^{-1}}\mathbb{I}_{\alpha 3} + \mathbb{I}_{3\beta}\mathrm{Ad}_{x_\beta^{-1}} + \mathbb{I}_{33} \tag{6.3}$$

is referred to as the locked moment of inertia. Recall that $\zeta_\alpha = x_\alpha^{-1}\dot{x}_\alpha$, and let $x = (x_1, x_2)$. Equation (6.2) can then be rewritten as

$$\mathbb{I}_{\mathrm{loc}}\,(\xi_3 + \mathcal{A}(x)\dot{x}) = 0. \tag{6.4}$$

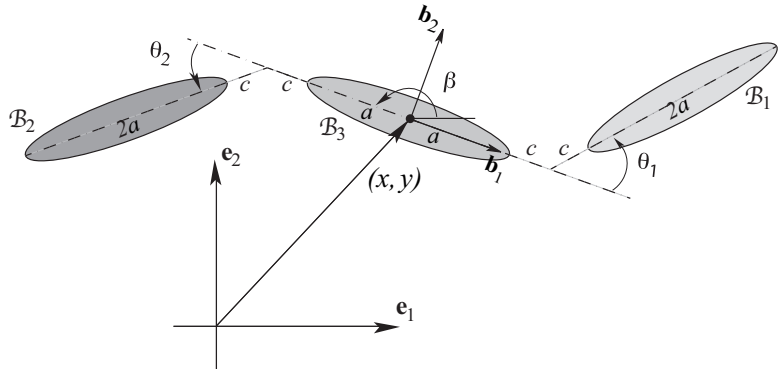

Fig. 4. A three-link mechanism submerged in a perfect fluid.

Here, the *local form of the connection* $\mathcal{A}$, as a function of the shape variables x, can be computed from the identity

$$\mathbb{I}_{\text{loc}}\,\mathcal{A}(x)\dot{x} = \left(\text{Ad}^{T}_{x_\alpha^{-1}}\mathbb{I}_{\alpha\beta} + \mathbb{I}_{3\beta}\right)\zeta_\beta. \tag{6.5}$$

For non-degenerate $\mathbb{I}_{\text{loc}}$, (6.4) is equivalent to

$$\xi_3 + \mathcal{A}(x)\dot{x} = 0, \tag{6.6}$$

which, in view of $\xi_3 = g_3^{-1}\dot{g}_3$, yields, using the terminology of Bloch, Krishnaprasad, Marsden, and Murray [1996], the following *reconstruction equation*:

$$\dot{g}_3 = -g_3\mathcal{A}(x)\dot{x}. \tag{6.7}$$

It is convenient for studying locomotion to assume that the relative motion x evolve according to prescribed functions of time.[6] The net locomotion g_3 is then fully determined by solving (6.7) and can be thought of as a geometric phase, or holonomy, over closed curves in $\mathfrak{X}$ traced by the shape variables (x_1, x_2); see Figure 3.

7. Swimming of a Three-Link Planar Mechanism

Consider the example analyzed in Radford [2003] of three articulated, submerged bodies that are constrained to undergo only planar motions, as shown in Figure 4.

A Planar Three-Link Fish. For concreteness, assume the three bodies are identical and made of a homogeneous material and have an ellipsoidal geometry. Let a denote the length of the major semi-axis of the ellipses and b denote the length of the minor semi-axis. Let the joints be placed a distance c away from the tips of the ellipses along their major axes, as shown in Figure 4.

[6] One can imagine that the joints are equipped with motors and controllers to enforce the prescribed motions. Of course, biological fish use their muscles to control their shape changes.

Consider a fixed inertial frame $\{\mathbf{e}_k\}$ and three body-fixed frames attached at the center of mass of each body, assumed to coincide with its geometric center. Let (β, x, y) denote the rigid motion of the middle ellipse relative to $\{\mathbf{e}_k\}$, and let θ_1 and θ_2 denote, respectively, the orientation of $\mathcal{B}_1$ and $\mathcal{B}_2$ relative to $\mathcal{B}_3$. One can readily verify that the motions x_α of $\mathcal{B}_1$ relative to $\mathcal{B}_3$ and $\mathcal{B}_2$ relative to $\mathcal{B}_3$ can be represented by

$$x_\alpha = \left(\begin{array}{cc|c} \cos\theta_\alpha & -\sin\theta_\alpha & \pm l(1+\cos\theta_\alpha) \\ \sin\theta_\alpha & \cos\theta_\alpha & \pm l\sin\theta_\alpha \\ \hline 0 & 0 & 1 \end{array}\right), \tag{7.1}$$

where the upper sign, i.e., the $(+)$, in $\pm$ is associated with θ_1, and $l = a+c$ is the distance between the mass center and the joint along the major semi-axis of the corresponding ellipse (see Figure 4). It should be clear from (7.1) that in this example the base space $\mathfrak{X}$ actually reduces to $S^1 \times S^1$, with coordinates $\theta = (\theta_1, \theta_2)$. Further, one may also verify that

$$\zeta_\alpha^T = (\dot\theta_\alpha, 0, \pm l\dot\theta_\alpha). \tag{7.2}$$

Two Approaches. We present two solutions to the planar three-link fish problem. In Section 7.1, we assume that the submerged bodies are *hydrodynamically decoupled*, as done in Radford [2003]. This assumption means that the added masses associated with a given body are not affected by the presence of the other bodies, which is clearly not true for a fish model. However, this assumption is useful for assessing qualitatively the behavior of the model, as analytical solutions are available. In Section 7.2, we accurately compute the added masses based on a boundary element method to obtain better quantitative estimates of the dynamics (see Figure 5).

7.1. Hydrodynamically Decoupled Bodies

Assume that the added masses associated with a given body are not affected by the presence of the other bodies. In this case, since the three ellipses are identical, one has

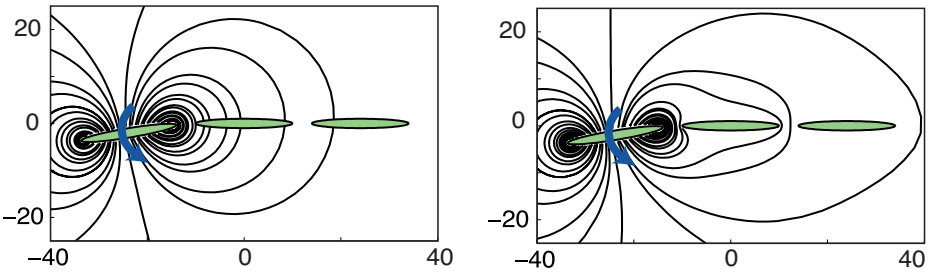

Fig. 5. Streamlines of the fluid velocity corresponding to a rotation of one of the ellipses with unit angular velocity—the direction of the rotation is indicated by the blue arrows. In (a), the three submerged ellipses are assumed to be hydrodynamically decoupled. This means that the motion of the fluid is not affected by the presence of the other two ellipses, which leads to the streamlines erroneously crossing the boundaries of these ellipses. In (b) the motion of the fluid is solved for numerically using a Boundary Element Method.

$\mathbb{I}_{11} = \mathbb{I}_{22} = \mathbb{I}_{33}$, with nonzero entries on the diagonal given by

$$j = I + I^f, \qquad m_1 = m + m_1^f, \qquad m_2 = m + m_2^f. \tag{7.3}$$

Here, I and m are the actual rotational and linear inertias of each rigid ellipse, with $I = m(a^2 + b^2)/4$, and I^f, m_1^f, and m_2^f are the added inertias due to the fluid whose values are given by (see, for example, Newman [1977, Chapter 4]),

$$I^f = \frac{1}{8}\rho_{\mathcal{F}}\pi(a^2 - b^2)^2, \qquad m_1^f = \rho_{\mathcal{F}}\pi b^2, \qquad m_2^f = \rho_{\mathcal{F}}\pi a^2. \tag{7.4}$$

Consequently, the locked moment of inertia $\mathbb{I}_{\text{loc}}$ and $\text{Ad}^T_{X_\alpha^{-1}}(\mathbb{I}_\alpha\zeta_\alpha)$ can readily be computed. One obtains

$$\mathbb{I}_{\text{loc}} = \left(\begin{array}{c|c} J & d^T \\ \hline d & M \end{array}\right), \tag{7.5}$$

where J is a scalar given by

$$J = 3j + l^2 m_2((1 + c_1)^2 + (1 + c_2)^2) + l^2 m_1(s_1^2 + s_2^2), \tag{7.6}$$

and d is given by

$$d = \begin{pmatrix} -lm_2(s_1 - s_2) - \frac{1}{2}l(m_2 - m_1)(S_1 - S_2) \\ lm_2(c_1 - c_2) + \frac{1}{2}l(m_2 - m_1)(C_1 - C_2) \end{pmatrix}, \tag{7.7}$$

while the 2×2 matrix M reads

$$M = \begin{pmatrix} m_1(1 + c_1^2 + c_2^2) + m_2(s_1^2 + s_2^2) & -\frac{1}{2}(m_2 - m_1)(S_1 + S_2) \\ -\frac{1}{2}(m_2 - m_1)(S_1 + S_2) & m_2(1 + c_1^2 + c_2^2) + m_1(s_1^2 + s_2^2) \end{pmatrix}. \tag{7.8}$$

The notation used in (7.6)–(7.8) is given by

$$\begin{array}{ll} c_\alpha = \cos\theta_\alpha, & s_\alpha = \sin\theta_\alpha, \\ C_\alpha = \cos(2\theta_\alpha), & S_\alpha = \sin(2\theta_\alpha). \end{array} \tag{7.9}$$

In addition, one finds that

$$\text{Ad}^T_{X_\alpha^{-1}}(\mathbb{I}_\alpha\zeta_\alpha) \;=\; \begin{pmatrix} j + l^2 m_2(1 + \cos\theta_\alpha) \\ \mp lm_2 \sin\theta_\alpha \\ \pm lm_2 \cos\theta_\alpha. \end{pmatrix} \dot{\theta}_\alpha. \tag{7.10}$$

To this end, one can obtain the local form of the connection $\mathcal{A}(\theta_\alpha)$ from (6.5) and solve (6.7) for the group motion g_3 of the three-link mechanism.

7.2. Hydrodynamically Coupled Bodies

To obtain accurate estimates of the motion, one needs to correctly solve for the fluid motion. Indeed, to compute the added inertias $\mathbb{M}_{ij}^f$ given in (3.15) where $\Theta_{ij}^{(\cdot)(\cdot)}$ are defined in (3.12)–(3.14), one has to solve for the velocity potentials $\boldsymbol{\chi}_i$ and $\boldsymbol{\varphi}_i$ of (3.8).

The Velocity Potentials. As we discussed in Section 3.1, the fluid velocity $\mathbf{u} = \nabla\phi$ is determined by solving Laplace's equation for the potential ϕ in the fluid domain $\mathcal{F}$

$$\Delta\phi = 0, \tag{7.11}$$

subject to the following boundary conditions:

$$\begin{cases} \nabla\phi \cdot \mathbf{n}_i = \mathbf{v}_i \cdot \mathbf{n}_i, & \text{on } \partial\mathcal{B}_i \\ \nabla\phi = 0, & \text{at } \infty. \end{cases} \tag{7.12}$$

This problem can be transformed, by superposition, into the problem of solving for the velocity potentials $\boldsymbol{\chi}_i$ and $\boldsymbol{\varphi}_i$ (see (3.8)). In the case of the planar three-link mechanism, let $\boldsymbol{\chi}_i = \chi_i\,\mathbf{b}_3$ and $\boldsymbol{\varphi}_i = \varphi_i^1\,\mathbf{b}_1 + \varphi_i^2\,\mathbf{b}_2$, where $\{\mathbf{b}_1, \mathbf{b}_2, \mathbf{b}_3\}$ denote the $\mathcal{B}_3$-fixed frame. Clearly, one has nine scalar potentials χ_i, φ_i^1, and φ_i^2, which are solutions to Laplace's equation subject to Neumann-type boundary conditions at their interface with the solid bodies; namely,

$$\begin{cases} \nabla\chi_i \cdot \mathbf{n}_i, = (\mathbf{b}_3 \times \mathbf{X}_i) \cdot \mathbf{n}_i & \text{on } \partial\mathcal{B}_i \\ \nabla\chi_i \cdot \mathbf{n}_j = 0, & \text{on } \partial\mathcal{B}_j,\ j \neq i, \end{cases} \tag{7.13}$$

and

$$\begin{cases} \nabla\varphi_i^\nu \cdot \mathbf{n}_i = \mathbf{b}_\nu \cdot \mathbf{n}_i, & \text{on } \partial\mathcal{B}_i \\ \nabla\varphi_i^\nu \cdot \mathbf{n}_j = 0, & \text{on } \partial\mathcal{B}_j,\ j \neq i, \end{cases} \tag{7.14}$$

where $\nu = 1, 2$. It should be clear from (7.13)–(7.14) that χ_i, φ_i^1, and φ_i^2 depend not only on the shape of $\mathcal{B}_i$ but also on the relative positions of the other two bodies with respect to $\mathcal{B}_i$.

The Numerical Method. The problem of solving Laplace's equation for χ_i, φ_i^1, and φ_i^2 over the fluid domain $\mathcal{F}$ subject to (7.13)–(7.14) can be replaced by an easier boundary value problem, which is then solved numerically using a boundary element method. The theoretical foundation of such methods is based on reformulating Laplace's equations as a boundary integral equation, using the divergence theorem (see Moran [1984, Chapter 8]). As a result, only the boundary surfaces of the submerged bodies need to be discretized; hence the computational advantages of such methods. We use the method devised by Smith and Hess [1966], which utilizes a piecewise-constant distribution of source singularities over the surfaces of the submerged bodies and computes this distribution as the solution of an integral equation. Physically speaking, this *fictitious* source distribution induces a velocity field in the fluid that is equivalent to the velocity field resulting from the motion of the submerged bodies.

The implementation of the method consists of the following steps:

1. The surface of each ellipse is discretized by n line segments, or panels.
2. A constant source density of unit strength is assigned along each panel. The use of source/sink distributions cannot contribute any net circulation and allows us to ensure a priori that there will not be any circulation anywhere in the fluid at all times.
3. The unit source density on each panel induces a velocity field everywhere in the fluid and, in particular, on the panels themselves. We compute the velocities induced by these unit source densities at the midpoint of each panel, called the control point; that is, we compute $n \times n$ induced velocity terms.

4. The source distribution is solved for by imposing appropriate boundary conditions on the normal velocities at the control points. More specifically, we solve for nine distinct source distributions corresponding to the nine sets of boundary conditions in (7.13)–(7.14).

For each source distribution, we compute the value of the corresponding potential function χ_i, φ_i^1, or φ_i^2 at the control points. By superposition, one can solve for the potential function ϕ due to arbitrary boundary conditions. In Figures 6 and 7, we plot the streamlines corresponding to the velocity field of the potential flow around various configurations and velocities of the submerged three-link mechanism.

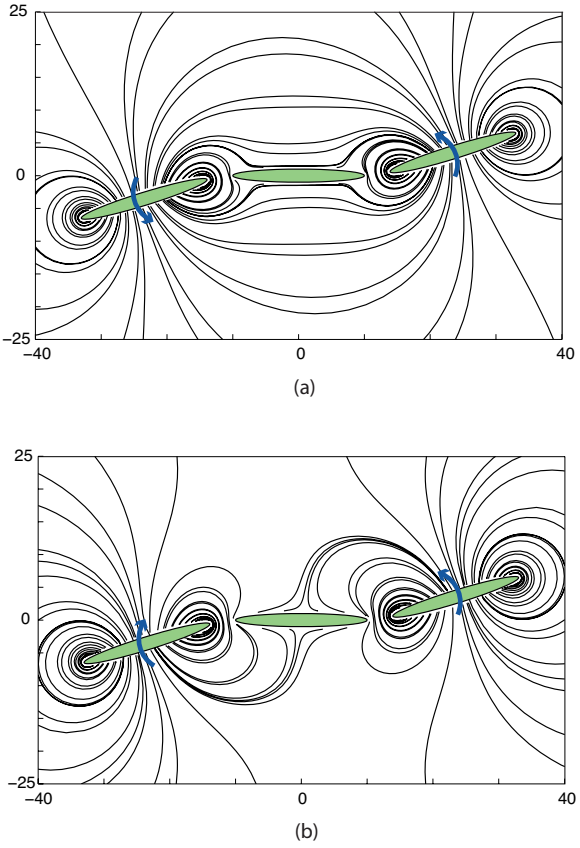

Fig. 6. Streamlines corresponding to two distinct velocity fields of the fluid associated with the same relative configuration of the three-link mechanism. In (a), the two outer ellipses are shown to rotate in the same direction relative to the center ellipse, while in (b) they are rotating in opposite directions. The direction of the rotation is indicated by the blue arrows.

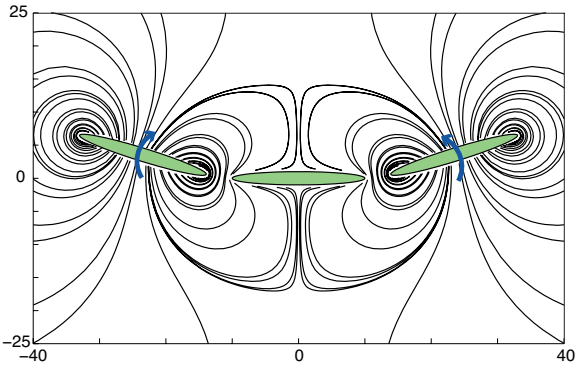

Fig. 7. The streamlines of the velocity field of the fluid for a given relative configuration of the three-link mechanism. The motion of the fluid is due to a motion of the three-link mechanism where the outer two ellipses are rotating in an opposite direction relative to the center ellipse. The direction of the rotation is indicated by the blue arrows.

Computing the Added Inertias. The added inertias are then calculated based on (3.12)–(3.14). Here, one has to compute six distinct added inertia matrices, namely, $\mathbb{M}^f_{11}$, $\mathbb{M}^f_{22}$, $\mathbb{M}^f_{33}$, $\mathbb{M}^f_{12}$, $\mathbb{M}^f_{13}$, and $\mathbb{M}^f_{23}$, each containing six independent components, due to the symmetry properties discussed in Section 3. It is worth emphasizing that, in our numerical scheme, the velocity potentials are computed directly relative to the $\mathcal{B}_3$-fixed frame. Consequently, the components of all six added masses $\mathbb{M}^f_{ij}$ are computed directly relative to the $\mathcal{B}_3$-fixed frame. In other words, the numerical scheme computes $\mathrm{Ad}^T_{x_\alpha^{-1}}\mathbb{M}^f_{\alpha\beta}\mathrm{Ad}_{x_\beta^{-1}}$ and $\mathrm{Ad}^T_{x_\alpha^{-1}}\mathbb{M}^f_{\alpha 3}$.[7]

7.3. Numerical Results and Discussion

We compute the net motion $g_3(t) = (\beta(t), x(t), y(t))$ of the articulated bodies due to prescribed periodic shape changes θ_1 and θ_2. Two solutions are presented: One corresponds to the hydrodynamically decoupled assumption, and one is based on accurately computing the added inertias. Interestingly, the former model results in smaller net travel than the latter, more accurate model.

Swimming of the Hydrodynamically Decoupled Bodies. Let $a = 10, b = 1, c = 2$, and $\rho_{\mathcal{F}} = 1/\pi$ and calculate the added inertias using (7.4). We first assume that $m = 0$, that is, the ellipses have zero inertias in a vacuum. The expressions for $\mathbb{I}_{\mathrm{loc}}$ and $\mathrm{Ad}^T_{x_\alpha^{-1}}(\mathbb{I}_\alpha\zeta_\alpha)$ given in (7.5) and (7.10) are used to compute the local form of the connection $\mathcal{A}(\theta)$ from

[7] Recall that, in (3.22), $\mathbb{M}^f_{ij}$ are expressed relative to the corresponding body-fixed frames, that is, for $i = j$, $\mathbb{M}^f_{ii}$ is expressed relative to the i^{th} body-fixed frame, and for $i \neq j$, $\mathbb{M}^f_{ij}$ is a two-point matrix with one leg in the i^{th}-frame and the second leg in the j^{th}-frame.

(6.5) by numerically inverting $\mathbb{I}_{\text{loc}}$. The result is substituted into (6.7) and a standard fourth-order Runge-Kutta integration scheme with constant time steps is used to obtain $g_3(t) = (\beta(t), x(t), y(t))$.

Swimming of the Hydrodynamically Coupled Bodies. The added inertias are computed for the same geometry of the three-link mechanism, as discussed in Section 7.2. The boundary of each ellipse is approximated using 50 line segments or panels. The added inertias are computed directly in the $\mathcal{B}_3$-fixed frame; hence, for the massless links, the the locked moment of inertia defined in (6.3) is just the sum of the computed added inertias. To compute $\mathcal{A}$ from (6.5), we first need to transform the relative velocities ζ_α to the $\mathcal{B}_3$-frame. Then, $\mathcal{A}$ is substituted into (6.7) to solve for the motion $g_3(t) = (\beta(t), x(t), y(t))$ using the same integration scheme employed for the hydrodynamically decoupled case. It is important to note that the added inertias are computed at each time step, that is, for each relative configuration of the three-link mechanism.

Massless Links. Figure 8 shows the solution $g_3(t) = (\beta(t), x(t), y(t))$ that is the result of the shape changes $\theta_1 = -\cos(t)$ and $\theta_2 = \sin(t)$. These shape functions produce a net forward motion of the three-link mechanism in the $(\mathbf{e}_1, \mathbf{e}_2)$-plane, as shown in Figure 8(a). In all figures, the solution corresponding to the hydrodynamically decoupled mechanism is depicted in dashed lines and that based on properly computing the added inertias is depicted in solid lines. In Figure 9, the three-link mechanism is shown to

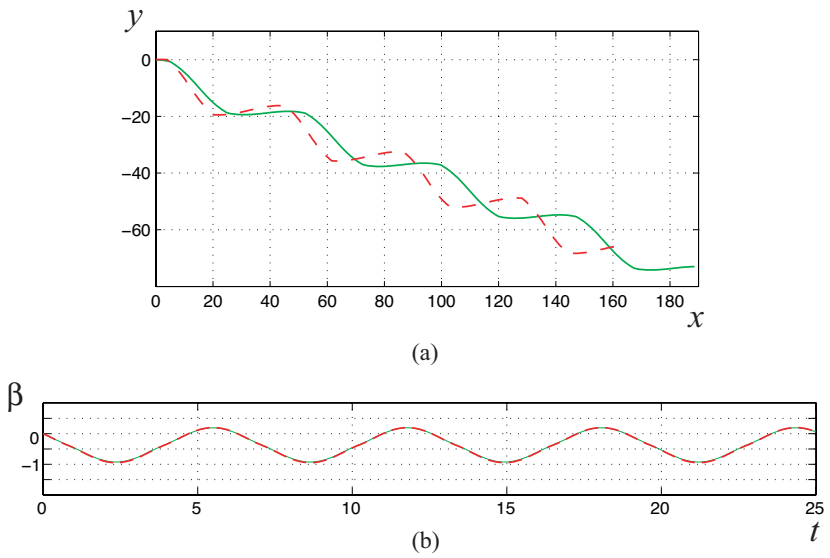

Fig. 8. Massless links: forward gait of the three-link mechanism due to the shape functions $\theta_1 = -\cos(t)$ and $\theta_2 = \sin(t)$. The trace of the mass center of $\mathcal{B}_3$ in the $(\mathbf{e}_1, \mathbf{e}_2)$ plane is plotted in (a), and the rotation angle $\beta(t)$ is shown in (b). Clearly, the mechanism oscillates as it propels itself but without undergoing a net rotation. The solid lines correspond to the motion based on computing the added inertias, while the dashed lines correspond to that of the hydrodynamically decoupled bodies.

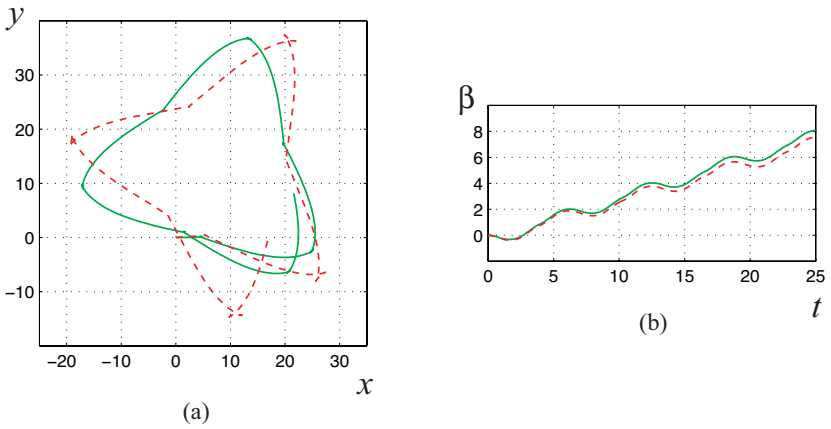

Fig. 9. Massless links: turning gait of the three-link mechanism due to the shape functions $\theta_1 = 1 - \cos(t)$ and $\theta_2 = -1 + \sin(t)$. The path that the mass center of $\mathcal{B}_3$ traces in the $(\mathbf{e}_1, \mathbf{e}_2)$ plane is plotted in (a) and the evolution of the rotation angle β as a function of time in (b). The solid lines correspond to the motion based on computing the added inertias, while the dashed lines correspond to that of the hydrodynamically decoupled bodies.

turn counterclockwise in the $(\mathbf{e}_1, \mathbf{e}_2)$ plane due to shape functions $\theta_1 = 1 - \cos(t)$ and $\theta_2 = -1 + \sin(t)$. The forward and turning gaits over one period $T = 2\pi$ of shape changes are shown in Figure 10.

Neutrally Buoyant Links. We now consider the case of neutrally buoyant, submerged ellipses with mass density equal to that of the fluid density $\rho_{\mathcal{F}}$. The body moment of inertia of each ellipse is $I = m(a^2 + b^2)/4$, where $m = \rho_{\mathcal{F}} \pi ab$ is the mass of the ellipse, and $\mathbb{M}_i^b$ has diagonal entries (I, m, m). Figures 11 and 12 depict the forward and turning motions due to $\theta_1 = -\cos(t)$, $\theta_2 = \sin(t)$ and $\theta_1 = 1 - \cos(t)$, $\theta_2 = -1 + \sin(t)$, respectively. One notices that the total distance travelled over one period of shape changes reduces considerably compared to Figures 8 and 9. This is expected because, given the same geometry and shape changes, the added inertias by the fluid are the same in this case as in the massless case. Yet, the total inertia is augmented by the actual inertia of the ellipses, and hence, the reason for the slower motion.

Although the model based on the hydrodynamically decoupled assumption captures qualitatively the correct dynamics, the results is this case are not based on realistic flows; see Figure 5. It is evident from the numerical examples in Figures 8 to 12 that accurately modeling the fluid motion has significant effects on the achieved net locomotion: The less accurate model results in smaller net travel.

Stopping the Actuation. Note that (θ_1, θ_2) are set into motion by applied torques (τ_1, τ_2) generated by motors located at the joints as described in equations (5.4). The coupling between (5.4) and (5.3) results in the net locomotion of the system. That is, given $(\tau_1(t), \tau_2(t))$, the shape motion $(\theta_1(t), \theta_2(t))$ and net locomotion $(\beta(t), x(t), y(t))$ are determined by solving the nonlinearly coupled system (5.3)–(5.4) or, alternatively,

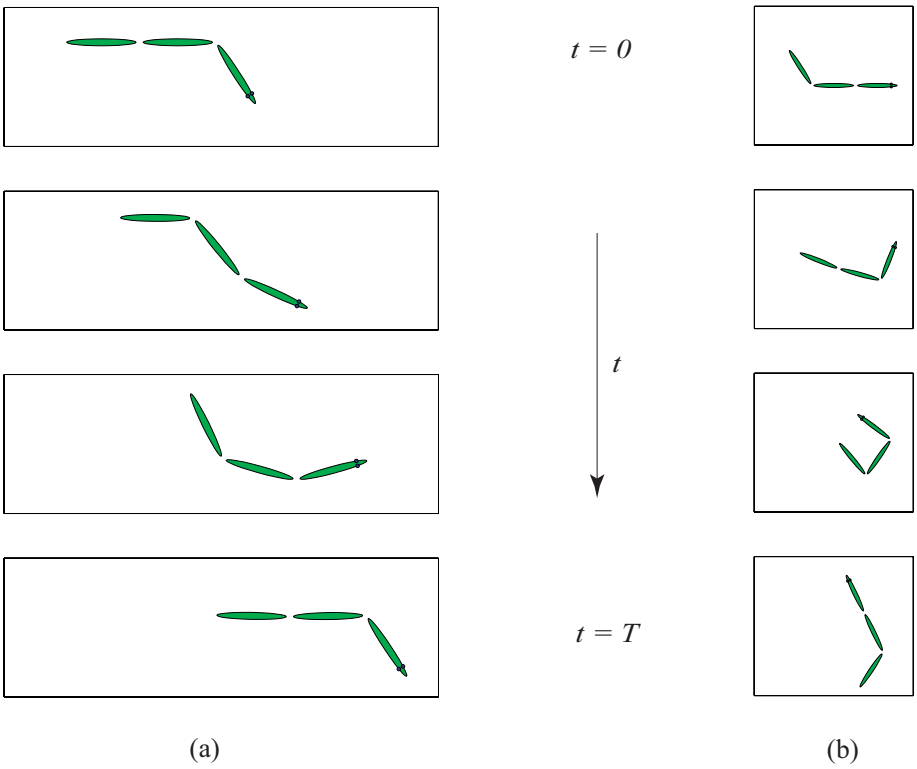

Fig. 10. (a) Forward gait of the three-link mechanism in the $(\mathbf{e}_1, \mathbf{e}_2)$-plane over one period $T = 2\pi$ due to shape changes $\theta_1 = -\cos(t)$ and $\theta_2 = \sin(t)$. (b) Turning gait over one period $T = 2\pi$ due to shape changes $\theta_1 = 1 - \cos(t)$ and $\theta_2 = -1 + \sin(t)$.

(6.7)–(5.4) since (5.3) is rewritten as (6.7). Assume that $(\tau_1(t), \tau_2(t))$ are prescribed such that for $t \geq t_c$ both torques are identically zero. By continuity, the motion for $t \geq t_c$ follows the initial value problem (no forcing) with initial conditions $(\beta(t_c), x(t_c), y(t_c), \theta_1(t_c), \theta_2(t_c))$. In other words, after t_c, the joints react *passively* to the surrounding fluid motion. Such investigation is very important to the study of gait generation and their stability, and will be addressed in future works.

Given $(\theta_1(t), \theta_2(t))$, one integrates (6.7) to obtain $(\beta(t), x(t), y(t))$, as done here, and uses (5.4) to compute the needed torques $(\tau_1(t), \tau_2(t))$. Now, assume that the three-link mechanism locks its shape at $t = t_c$, that is, set both $(\dot{\theta}_1(t_c), \dot{\theta}_2(t_c))$ and $(\ddot{\theta}_1(t_c), \ddot{\theta}_2(t_c))$ equal to zero. Based on (6.7), the motion $(\beta(t), x(t), y(t))$ and, hence, the fluid motion stop instantaneously at $t = t_c$. Of course, the torques needed to achieve this must be infinite (a Dirac function at $t = t_c$) in order for the body to generate instantaneously a *finite amount of work equal and opposite to the work done during the interval* $[t_0, t_c]$.

Motion Planning. Direct numerical simulation allows one to demonstrate the ability of a system of articulated bodies to propel itself in a fluid due to periodic motion of the shape variables. By itself, this is insufficient for *designing such trajectories or gaits*. One would

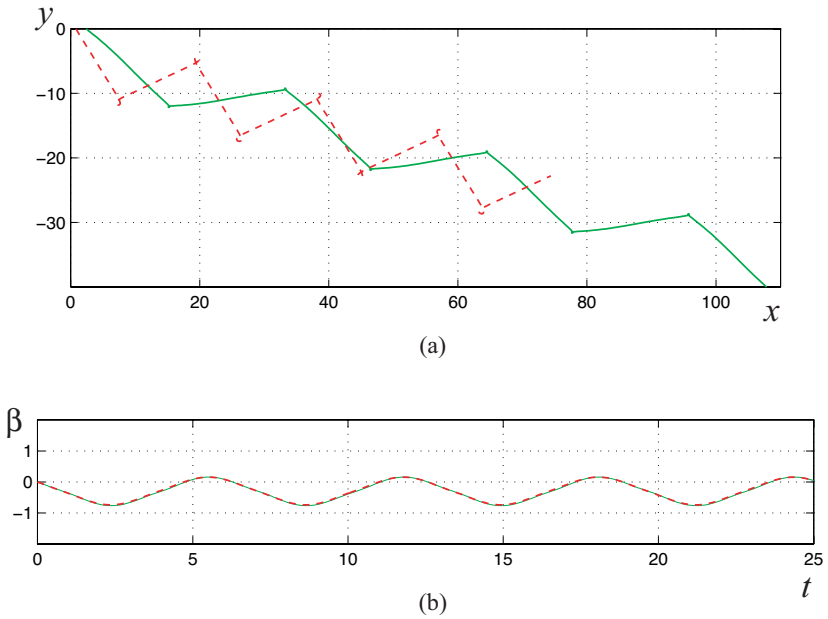

Fig. 11. Neutrally buoyant links: forward gait due to the shape functions $\theta_1 = -\cos(t)$ and $\theta_2 = \sin(t)$. The solid lines in (b) correspond to the motion based on computing the added inertias, while the dashed lines correspond to that of the hydrodynamically decoupled bodies.

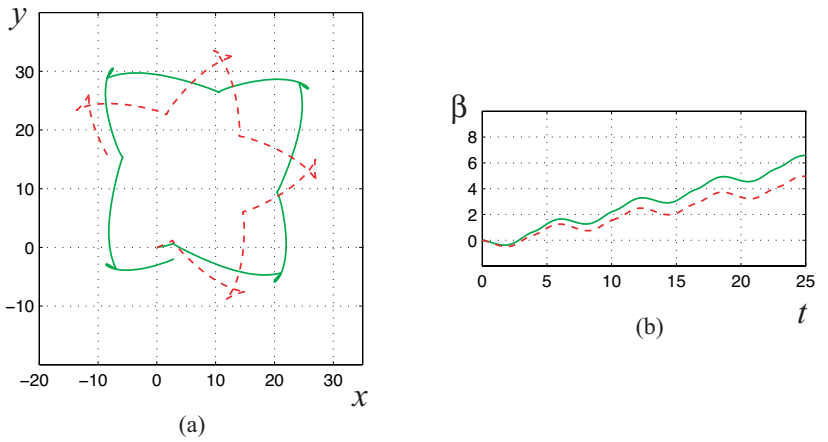

Fig. 12. Neutrally buoyant links: turning gait due to the shape functions $\theta_1 = 1-\cos(t)$ and $\theta_2 = -1 + \sin(t)$. The solid lines correspond to the motion based on computing the added inertias, while the dashed lines correspond to that of the hydrodynamically decoupled bodies.

need a rigorous foundation for the selection of patterns of shape changes that produce desired motion. Indeed, motion planning and control of self-propelled underwater robotic vehicles have been the subjects of serious studies recently, and some advances have been made in the case of *local* motion planning. In particular, in Radford and Burdick [1998], a *local* expression for the solution $g_3(t)$ is written as a function of the hydrodynamically decoupled connection $\mathcal{A}$ and its curvature in the case of *small* periodic shape changes. Other important papers in this direction are Cortés, Martínez, Ostrowski, and McIsaac [2001] and Ostrowski, Desai, and Kumar [2000]; see also references therein. *In the present work, the assumption of small shape changes was not required for computing the connection* $\mathcal{A}$. Also, because the dependence of the added inertias on the shape variables is computed numerically, an analytic expression for $\mathcal{A}$ is not required and, in any case, is probably difficult or impossible to obtain. One could devise a method to numerically compute the curvature of A and use results from holonomy to obtain insight into trajectory design. These ideas will be pursued in a future work.

Three-Dimensional Effects. The generalization of the two-dimensional numerical results to the three-dimensional problem (described in Sections 2 through 6) is crucial for understanding the behavior of biological fish. In the three-dimensional case, one expects the added mass effects to decrease. Indeed, the two-dimensional assumption is based on considering both the fluid and the submerged solids to have *very large* (infinite) width. Consequently, the added mass effects, which are proportional to the amount of fluid pushed by the moving bodies, are larger in the two-dimensional case than in the more realistic three-dimensional models that properly encode the width of the solids. By the same argument, one would expect the three-dimensional added mass effects to be more important for fish with large aspect-ratio tails like tuna and carangiform fish in general than for slender anguilliform fish like eels.

8. Concluding Remarks and Future Directions

We have considered the problem of N solid bodies submerged in an ideal fluid in the context of studying the swimming of a class of aquatic animals—namely, fish that propel and steer themselves by coupling their shape changes with fluid dynamic effects.

The problem of N submerged, neutrally buoyant bodies is described in a general setting, and then a reduced model for the dynamics is obtained following a two-stage reduction process. The first reduction exploits the symmetry associated with the conservation of circulation of the fluid. The underlying assumption is that the motion of the solids does not generate circulation (although we plan to include other effects such as point vortices in future models). As a result, the effects of the fluid may be included *without explicitly incorporating the fluid variables*. In particular, the reduced configuration space for potential flows is identified with the configuration space $\mathcal{R}$ of the solid bodies. The kinetic energy of the system is then expressed as a function on the tangent bundle $T\mathcal{R}$. The added inertias, which are boundary integral functions of the fluid density and bodies configuration, account for the effect of the fluid.

The symmetry of the system of bodies and fluid under superimposed rigid body motions is exploited by establishing a connection on $\mathcal{R}$. The net locomotion of the

system is then realized as the sum of geometric and dynamic phases over the shape space consisting of allowable relative motions, or deformations, of the bodies. In particular, the reconstruction equations that govern the net locomotion at zero momentum, that is, the geometric phases, are explicitly derived.

As an illustrative example, we studied the motion of a submerged planar three-link mechanism. The mechanism is shown to propel and steer itself at zero momentum due to periodically changing its shape. The added inertias are calculated based on a boundary element method. The resultant models predict a much larger net travel than models assuming hydrodynamically decoupled links.

Future Directions. There is a need to establish a rigorous foundation for selecting patterns of shape changes that produce a desired net locomotion. By viewing the trajectories of the net motion as geometric phases, or holonomy, over closed curves in the shape space, the net motion is dictated by the curvature of the connection, which has to be computed numerically. To this picture, one needs to add locomotion due to dynamic phases and address the issue of trajectory generation as a result of both geometric and dynamic phases. One approach would be to properly define one or several functions that measure the efficiency of the mechanism in moving between two given points in the ambient fluid. The problem of trajectory generation can then be formulated as an optimization problem that maximizes/minimizes such functions (Kanso and Marsden [2005]). Indeed, biological fish change their behavior depending on the conditions in which they swim. When swimming peacefully, their concern is to minimize their energy cost, but if attacked by a predator, their energy concerns become secondary as they speed to escape.

A second aspect of the problem of studying propulsion of aquatic animals lies in analyzing their interaction with self-generated vortices as well as vortices shed by other objects. In their natural environment, aquatic animals contend with the presence of vortices due to various sources. In addressing this problem, a reduced model will be derived for the solid bodies submerged in an ideal, incompressible fluid and interacting with point vortices. This assumption is reasonable given that the mechanism of vortex shedding that takes place, say, in the thin boundary layer around the fish can be neglected. In this case, the bulk of the fluid remains effectively ideal. As a first step towards studying the interaction with vortices, we put a deformable cloth on the three-link fish to cover the joints, hence preventing the fluid particles from passing through the joints and drawing the model closer to that of an elastic fish. The interested reader is referred to the website *http://www.cds.caltech.edu/∼marsden/research/demos/* for further details and illustrations.

Appendix A. The Group of Rigid Motions

The group of rigid body motion $G = \mathrm{SE}(3)$ is a Lie group, that is, a manifold endowed with a smooth, associative, and invertible binary operation called the group multiplication. For a general introduction to Lie groups, see, e.g., Chapter 9 of Marsden and Ratiu (1999). An element of SE(3) is given by $(R, \mathbf{r})$ where $R \in \mathrm{SO}(3)$ is a rotation matrix that describes the orientation of the rigid body and $\mathbf{r} \in \mathbb{R}^3$ describes its position relative

to a fixed inertial frame. That is, if $\mathbf{x}$ and $\mathbf{X}$ are the position vectors of the same material point described, respectively, relative to an inertial frame $\{\mathbf{e}_k\}$ and a body-fixed frame $\{\mathbf{b}_k\}$, one has

$$\begin{pmatrix}\mathbf{x}\\1\end{pmatrix} = \begin{pmatrix}R & \mathbf{r}\\0 & 1\end{pmatrix}\begin{pmatrix}\mathbf{X}\\1\end{pmatrix} = \begin{pmatrix}R\,\mathbf{X}+\mathbf{r}\\1\end{pmatrix}. \tag{A.1}$$

In this representation, the group operation corresponds to matrix multiplication. The identity element of G is denoted by e and is equal to $(I, (0, 0, 0))$, where I is the 3×3 identity matrix. One can readily calculate the inverse $g^{-1} = (R, \mathbf{r})^{-1}$ of an element $g = (R, \mathbf{r}) \in G$,

$$\begin{pmatrix}\mathbf{X}\\1\end{pmatrix} = \begin{pmatrix}R^T x - R^T\mathbf{r}\\1\end{pmatrix} = \begin{pmatrix}R^T & -R^T\mathbf{r}\\0 & 1\end{pmatrix}\begin{pmatrix}\mathbf{x}\\1\end{pmatrix}. \tag{A.2}$$

The action of G on a manifold Q, which in particular may be the group itself, is a map Φ: $G \times Q \to Q$ such that $(g, q) \to \Phi_g(q)$. The left, respectively right, action $\Phi^L_g(q) = gq$, respectively $\Phi^R_g(q) = qg$, is defined such that $\Phi^L_{hg}(q) = (hg)q = h(gq) = \Phi^L_h(gq)$, respectively, $\Phi^R_{gh}(q) = q(gh) = (qg)h = \Phi^R_h(gq)$. The conjugation map Φ^C: $G \times G \to G$ defined as $\Phi^C_g(h) = ghg^{-1}$ is of particular importance.

A Lie algebra is a vector space endowed with a skew-symmetric, bilinear operation, called the Lie bracket, which satisfies the Jacobi identity. In general, any Lie group has a natural Lie algebra defined by the space of left, or right, invariant vector fields[8] endowed with the Jacobi-Lie bracket. The reader is reminded that the Jacobi-Lie bracket is equivalent to the commutator of vector fields. Further, note that the vector space defining the Lie algebra is isomorphic to the tangent space of the Lie group at the identity element, i.e., T_eG. In particular, the elements of the Lie algebra $\mathfrak{g}$ of the group of rigid motion G are defined by

$$\xi(t) = \left.\frac{\mathrm{d}}{\mathrm{d}s}\right|_{s=0} h(t)^{-1}\, h(t+s), \tag{A.3}$$

where $h \in G$. One can readily verify that $\xi(t)$ is equal to $\big(\boldsymbol{\Omega}(t), \mathbf{v}(t)\big)$; that is, it represents the angular and translational velocities of the rigid body with respect to the body-fixed frame and can be written in matrix form as follows:

$$\xi = \begin{pmatrix}\hat{\Omega} & \mathbf{v}\\0 & 0\end{pmatrix}, \tag{A.4}$$

where the $\hat{}$ operator is defined in Section 3. Further, note that $\xi = h^{-1}\dot{h}$ is left-invariant since

$$\Big(\Phi^L_g(h)\Big)^{-1}\dot{\Big(\Phi^L_g(h)\Big)} = (gh)^{-1}(g\dot{h}) = h^{-1}g^{-1}g\dot{h} = h^{-1}\dot{h}. \tag{A.5}$$

The adjoint action of G on $\mathfrak{g}$ Ad: $G \times \mathfrak{g} \to \mathfrak{g}$ is defined as the derivative at the identity of the conjugation map Φ^C, i.e., $\mathrm{Ad}_g\xi \equiv T_e\Phi^C$, that is,

$$\mathrm{Ad}_g\xi = g\xi g^{-1}. \tag{A.6}$$

[8] That is, vector fields that are invariant under the left, or right, action of the group on itself.

It is useful to calculate an explicit expression for the adjoint map Ad. In order to do this, we write (A.6) as follows:

$$\mathrm{Ad}_g\xi = \begin{pmatrix} R & \mathbf{r} \\ 0 & 1 \end{pmatrix} \begin{pmatrix} \hat{\Omega} & \mathbf{v} \\ 0 & 0 \end{pmatrix} \begin{pmatrix} R^T & -R^T\mathbf{r} \\ 0 & 1 \end{pmatrix}. \tag{A.7}$$

Finally, one can readily verify that (A.7) can be written as

$$\mathrm{Ad}_g\xi = \begin{pmatrix} R & 0 \\ \hat{r}R & R \end{pmatrix} \begin{pmatrix} \mathbf{\Omega} \\ \mathbf{v} \end{pmatrix}, \tag{A.8}$$

where ξ is expressed as an element in $\mathbb{R}^6$ (as in (3.19)) and the adjoint action Ad_g as a 6×6 matrix. For more details on this calculation, see, e.g., Chapter 2 of Murray and Sastry (1994).

Given the Lie group G with its Lie algebra $\mathfrak{g}$, and given the action Φ of G on a manifold Q, then, associated with each element $\xi \in \mathfrak{g}$, one gets a vector field ξ_Q on Q defined by

$$\xi_Q(q) = \left.\frac{\mathrm{d}}{\mathrm{d}t}\right|_{t=0} \Phi_{e^{\xi t}}(q), \tag{A.9}$$

where $e^{\xi t}$ is the exponential map. The vector field ξ_Q is referred to as the infinitesimal generator. In particular, the infinitesimal generator of the conjugation action of G on itself is referred to as the adjoint action of the Lie algebra on itself, denoted as ad_ξ, and corresponds to the Jacobi-Lie bracket. For the group of rigid motion SE(3), the reader can readily verify that the adjoint action ad_ξ is given by

$$\mathrm{ad}_\xi = \begin{pmatrix} \hat{\Omega} & 0 \\ \hat{v} & \hat{\Omega} \end{pmatrix}. \tag{A.10}$$

Note that, in general, any representation of a Lie group G on a vector space V similarly induces a representation of G on the dual space V^*. Specifically, one can also define a coadjoint action Ad^* of G on $\mathfrak{g}^*$, the dual of the Lie algebra, as well as a coadjoint map ad^*: $\mathfrak{g}^* \to \mathfrak{g}^*$, such that $\langle \delta, \mathrm{ad}_\xi \eta \rangle = \langle \mathrm{ad}^*_\xi \delta, \eta \rangle$, where $\delta \in \mathfrak{g}^*$ and $\langle , \rangle$ represents the pairing between $\mathfrak{g}$ and $\mathfrak{g}^*$.

To conclude this review, we discuss SE(2), the subgroup of SE(3) that corresponds to planar rigid body motion, and its Lie algebra $\mathfrak{se}(2)$, see, e.g., Chapter 2 of Kelly (1998). In this case, one may represent elements of $SE(2)$ by (β, x, y), where β is the orientation of the body relative to an inertial frame and (x, y) are the coordinates of a given material point of the body (this is illustrated in Figure 4 for $\mathcal{B}_3$). Further, elements of $\mathfrak{se}(2)$ may be represented as $\eta = (\Omega_\beta, v_x, v_y)$, where, clearly, Ω_β is the angular velocity and (v_x, v_y) is the translational velocity. The conjugation map as well as the adjoint actions are defined in a similar way as above.

B. Principal Bundles, Connections, and Reduction

In this appendix, we derive formally some of the results presented in Sections 4 and 5.

The Bundle Structure. We first show that $\mathcal{R}$ is a principal bundle with structure group G and diagonal action of G on $\mathcal{R}$, $G \times \mathcal{R} \to \mathcal{R}$, given by $h(g_1, g_2, g_3) = (hg_1, hg_2, hg_3)$; we do this following Cendra and Marsden (2004), which encountered a similar structure for the case of asteroid pairs. Remember that $\mathcal{R}$ is said to form a principal bundle if there exists a free (left) action $G \times \mathcal{R} \to \mathcal{R}$ of a Lie group G, such that the natural projection $\pi\colon \mathcal{R} \to \mathcal{R}/G$ is a submersion. Let $\mathfrak{X} = G \times G$ be the base space and $\pi\colon \mathcal{R} \to \mathfrak{X}$ be the projection map given by

$$(x_1, x_2) = \pi(g_1, g_2, g_3) = (g_3^{-1} g_1, g_3^{-1} g_2). \tag{B.1}$$

The map π can be interpreted physically as a representation of the rigid motions of $\mathcal{B}_1$ and $\mathcal{B}_2$ relative to a body-fixed frame attached to $\mathcal{B}_3$ (see Figure 2).

Sections and Connections. Consider the section $\sigma : \mathfrak{X} \to \mathcal{R}$ of the bundle π given by

$$\sigma(x_1, x_2) = (x_1, x_2, e). \tag{B.2}$$

This shows that $\pi : \mathcal{R} \to \mathfrak{X}$ is a trivial principal bundle, i.e., $\mathcal{R} = \mathfrak{X} \times G$. Further, for any $a \in G$, one has a section $a\sigma(x_1, x_2) = (a\,x_1, a\,x_2, a)$. The one-parameter family of these sections gives a foliation of the space $T\mathcal{R}$. The tangent distribution to this foliation defines a principal connection on $\mathcal{R}$. Indeed, an element of this distribution

$$v = \big(a\,x_1,\ a\,x_2,\ a,\ \dot{a}\,x_1 + a\,\dot{x}_1,\ \dot{a}\,x_2 + a\,\dot{x}_2,\ \dot{a}\big) \tag{B.3}$$

can naturally be split into a horizontal vector

$$v^{\mathrm{h}} = \big(a\,x_1,\ a\,x_2,\ a,\ a\,\dot{x}_1,\ a\,\dot{x}_2,\ 0\big), \tag{B.4}$$

and a vertical vector

$$v^{\mathrm{v}} = \big(a\,x_1,\ a\,x_2,\ a,\ \dot{a}\,x_1,\ \dot{a}\,x_2,\ \dot{a}\big). \tag{B.5}$$

Hence, the principal connection is characterized by the horizontal and vertical subspaces whose vectors are of the form (B.4) and (B.5), respectively, or equivalently, by the connection one-form $A : T\mathcal{R} \to \mathfrak{g}$ given by

$$A(g_1, g_2, g_3, \dot{g}_1, \dot{g}_2, \dot{g}_3) = \mathrm{Ad}_{g_3}\xi_3. \tag{B.6}$$

Reduced Dynamics. Given that the Lagrangian in (3.22) is invariant under the left action of G on $\mathcal{R}$, a reduced variational principle, without any reference to a connection on $\mathcal{R}$, can be stated, and the corresponding reduced Euler-Lagrange equations can be derived on $T\mathcal{R}/G$. However, due to the existence of A on $\mathcal{R}$, we realize the space $T\mathcal{R}/G$ in a way that leads to an interesting form of these equations, then called Lagrange-Poincaré equations; see Cendra, Marsden, and Ratiu (2001).

The Space $\mathfrak{X} \times \mathfrak{g} \times \mathfrak{g} \times \mathfrak{g}$**.** Using the connection A given by (B.6), one can introduce the bundle isomorphism[9]

$$\alpha_A\colon T\mathcal{R}/G \to T\mathfrak{X} \oplus \tilde{\mathfrak{g}}, \tag{B.7}$$

[9] Notice that the bundles $T\mathcal{R}/G$ and $T\mathfrak{X} \oplus \tilde{\mathfrak{g}}$ do not depend on the connections, but the map α_A does.

where $\tilde{\mathfrak{g}} \equiv (\mathcal{R} \times \mathfrak{g})/G$ is the adjoint bundle associated with the principal bundle $\pi : \mathcal{R} \to \mathfrak{X} \equiv \mathcal{R}/G$ and the adjoint action of the group G on the vector space $\mathfrak{g}$. That is, a typical element of $\tilde{\mathfrak{g}}$ is written as $[(g_1, g_2, g_3, \xi)]_G$, where the equivalence class $[(\cdot)]_G$ is defined by $[(g_1, g_2, g_3, \xi)]_G \equiv \{(hg_1, hg_2, hg_3, \mathrm{Ad}_h\, \xi) : h \in G\}$. The isomorphism α_A of (B.7) is given by

$$\alpha_A\big([(g_1, g_2, g_3, \dot{g}_1, \dot{g}_2, \dot{g}_3)]_G\big) = T\pi(g_1, g_2, g_3, \dot{g}_1, \dot{g}_2, \dot{g}_3) \oplus [(g_1, g_2, g_3), A(g_1, g_2, g_3, \dot{g}_1, \dot{g}_2, \dot{g}_3)]_G, \quad \text{(B.8)}$$

where

$$T\pi(g_1, g_2, g_3, \dot{g}_1, \dot{g}_2, \dot{g}_3) = (x_1, x_2, \dot{x}_1, \dot{x}_2), \quad \text{(B.9)}$$

and

$$\begin{aligned}[(g_1, g_2, g_3), A(g_1, g_2, g_3, \dot{g}_1, \dot{g}_2, \dot{g}_3)]_G &= [(g_1, g_2, g_3), \mathrm{Ad}_{g_3}\xi_3]_G, \\ &= [(g_3^{-1}g_1, g_3^{-1}g_2, e), \xi_3]_G, \\ &= [(x_1, x_2, e), \xi_3]_G.\end{aligned} \quad \text{(B.10)}$$

Now, one can naturally identify $(x_1, x_2, \dot{x}_1, \dot{x}_2) \equiv (x_1, x_2, \zeta_1, \zeta_2)$, where $\zeta_{1,2}$ are defined in Section 5.1 That is, one identifies $T\mathfrak{X} \equiv \mathfrak{X} \times \mathfrak{g} \times \mathfrak{g}$. Further, one can identify $[(x_1, x_2, e), \xi_3]_G \equiv (x_1, x_2, \xi_3)$. Hence, the bundle $\tilde{\mathfrak{g}}$ becomes simply $\tilde{\mathfrak{g}} \equiv \mathfrak{X} \times \mathfrak{g}$. It follows from these identifications that

$$T\mathfrak{X} \oplus \tilde{\mathfrak{g}} \equiv \mathfrak{X} \times \mathfrak{g} \times \mathfrak{g} \times \mathfrak{g}. \quad \text{(B.11)}$$

As a result, the Lagrangian L_R in (3.22) is rewritten as a function l on $\mathfrak{R} = \mathfrak{X} \times \mathfrak{g} \times \mathfrak{g} \times \mathfrak{g}$, and the Lagrange-Poincaré equations are derived on this space using reduced variations, as done in Section 5.2.

Reduced Variations. By definition, ζ_α and ξ_3, as well as ξ_α all take the form $\gamma = y^{-1}\dot{y}$, and hence the variations $\delta\zeta_1$, $\delta\zeta_2$, and $\delta\xi_3$ follow the same expression; namely,

$$\delta\gamma = \dot{\eta} + [\gamma, \eta], \quad \text{(B.12)}$$

where $\eta = y^{-1}\delta y$. In order to prove (B.12), one considers an arbitrary variation δy and calculates the variation it induces on $\delta\gamma$, namely,

$$\delta\gamma = \delta(y^{-1}\dot{y}) = \delta(y^{-1})\dot{y} + y^{-1}\delta\dot{y}. \quad \text{(B.13)}$$

Recall that $y^{-1}y = e$, where e is the identity, and hence $\delta(y^{-1}y) = 0$, which implies $\delta y^{-1} = -y^{-1}(\delta y)y^{-1}$. On the other hand, the time derivative and δ commute, and

$$y^{-1}\delta\dot{y} = \mathrm{d}(y^{-1}\delta y)/\mathrm{d}t - \big(\mathrm{d}(y^{-1})/\mathrm{d}t\big)\delta y.$$

Substitute these identities back into (B.13) to get the result in (B.12).

Acknowledgments

This research was partially supported by NSF-ITR grant ACI-0204932 and ONR Contract N00014-02-1-0826. We are grateful to Joel Burdick, Scott Kelly, Jim Radford, and Banavara Shashikanth for their useful comments and inspiration over the years.

References

Arnold, V. I. [1966], Sur la géométrie differentielle des groupes de Lie de dimenson infinie et ses applications à l'hydrodynamique des fluids parfaits, *Ann. Inst. Fourier, Grenoble* **16**, 319–361.

Bloch, A. M., P. S. Krishnaprasad, J. E. Marsden, and R. M. Murray [1996], Nonholonomic mechanical systems with symmetry, *Arch. Rat. Mech. Anal.* **136(1)**, 21–99.

Borelli, G. [1989], *On the Movement of Animals,* Springer-Verlag, Heidelberg.

Borisov, A. V., and I. S. Mamaev [2003], An integrability of the problem on motion of cylinder and vortex in the ideal fluid, *Reg. Chaotic Dynam.* **8**, 163–166.

Cendra, H., and J. E. Marsden [2004], The dynamics of asteroid pairs, *preprint*.

Cendra, H., J. E. Marsden, and T. S. Ratiu [2001], *Lagrangian reduction by stages*, vol. 152 of *Memoirs*, American Mathematical Society, Providence, R.I.

Chorin, A. J., and J. E. Marsden [1979], *A Mathematical Introduction to Fluid Mechanics,* Springer-Verlag, New York.

Cortés, J., S. Martínez, J. P. Ostrowski, and K. A. McIsaac [2001], Optimal gaits for dynamic robotic locomotion, *Intern. J. Robotics Research*, **20**, 707–728.

Coutand, D., and S. Shkoller [2004], Motion of an elastic solid inside of an incompressible viscous fluid, *Arch. Rational Mech. Anal.*, **176**(1), 25–102.

Ebin, D. G., and J. E. Marsden [1969], Groups of diffeomorphisms and the solution of the classical Euler equations for a perfect fluid, *Bull. Amer. Math. Soc. (N.S.)* **75**, 962–967.

Kanso, E. and J.E. Marsden [2005], Optimal motion of an articulated body in a perfect fluid (submitted).

Kelly, S. D. [1998], *The Mechanics and Control of Robotic Locomotion with Applications to Aquatic Vehicles*, Ph.D. thesis, California Institute of Technology.

Lamb, H. [1932], *Hydrodynamics*. 6 ed. Dover, NY.

Leonard, N. E. [1997], Stability of a bottom-heavy underwater vehicle, *Automatica* **33**, 331–346.

Liao, J. C., D. N. Beal, G. V. Lauder, and M. S. Triantafyllou [2003a], Fish exploiting vortices decrease muscle activity, *Science*, **302**, 1566–1569.

Liao, J. C., D. N. Beal, G. V. Lauder, and M. S. Triantafyllou [2003b], The Kármán gait: Novel body kinematics of rainbow trout swimming in a vortex street, *J. Exp. Biol.*, **206**, 1059-1073.

Lighthill, J. [1975], *Mathematical Biofluiddynamics*. Society for Industrial and Applied Mathematics, PA.

Marsden, J. E. [1992], *Lectures on Mechanics*, vol. 174 of *London Math. Soc. Lecture Note Ser.* **174**. Cambridge University Press.

Marsden, J., G. Misiolek, J. P. Ortega, M. Perlmutter, and T. Ratiu [2005], *Hamiltonian reduction by stages*. Springer Lecture Notes in Mathematics, Springer-Verlag, Heidelberg (to appear).

Marsden, J. E., S. Pekarsky, S. Shkoller, and M. West [2001], Variational methods, multisymplectic geometry and continuum mechanics, *J. Geometry Physics* **38**, 253–284.

Marsden, J. E., and T. S. Ratiu [1999], *Introduction to Mechanics and Symmetry*, vol. 17 of *Texts in Applied Mathematics*, vol. 17; 1994, 2d ed., 1999. Springer-Verlag, New York.

Marsden, J. E., T. S. Ratiu, and J. Scheurle [2000], Reduction theory and the Lagrange-Routh equations, *J. Math. Phys.* **41**, 3379–3429.

Marsden, J. E., and J. Scheurle [1993], Lagrangian reduction and the double spherical pendulum, *ZAMP* **44**, 17–43.

Marsden, J. E., and A. Weinstein [1983], Coadjoint orbits, vortices and Clebsch variables for incompressible fluids, *Physica D* **7**, 305–323.

Mason, R., and J. W. Burdick [2000], Experiments in carangiform robotic fish locomotion. In *Proc. IEEE Int. Conf. Robotics and Automation*, pp. 428–435.

Moran, J. [1984], *An Introduction to Theoretical and Computational Aerodynamics.* John Wiley & Sons, New York.

Morgansen, K. A., V. Duindam, R. J. Mason, J. W. Burdick, and R. M. Murray [2001], Nonlinear control methods for planar carangiform robot fish locomotion. In *Proc. IEEE Int. Conf. Robotics and Automation*, pp. 427–434.

Müller, U. K. [2003], Fish'n Flag, *Science* **302**, pp. 1511–1512.

Murray, R., Z. Li, and S. Sastry [1994], *A Mathematical Introduction to Robotic Manipulation*. CRC Press, Boca Raton, FL.

Newman, J. N. [1977], *Marine Hydrodynamics*. MIT Press, Cambridge, MA.

Newman, J. N., and T. Y. Wu [1975], Hydrodynamical aspects of fish swimming. In T. Wu, C. Brokaw, and C. Brennen, editors, *Swimming and Flying in Nature* **2**, pp. 615–634. Plenum Press, NY.

Oh, Y. G., N. Sreenath, P. S. Krishnaprasad, and J. E. Marsden [1989], The dynamics of coupled planar rigid bodies. Part 2: Bifurcations, periodic solutions and chaos, *Dynam. Diff. Eq.* **1**, 269–298.

Ostrowski, J. P., J. P. Desai, and V. Kumar [2000], Optimal gait selection for nonholonomic locomotion systems, *Intern. J. Robotics Research*, **19**, 225–237.

Radford, J. [2003], *Symmetry, Reduction and Swimming in a Perfect Fluid*, Ph.D. thesis, California Institute of Technology.

Radford, J., and J. Burdick [1998], Local motion planning for nonholonomic control systems evolving on principal bundles. In *Proc. Math. Theory of Networks and Systems*.

Shashikanth, B. N., J. E. Marsden, J. W. Burdick, and S. D. Kelly [2002], The Hamiltonian structure of a 2D rigid circular cylinder interacting dynamically with N point vortices, *Phys. Fluids* **14**, 1214–1227.

Smith, A. M. O., and J. L. Hess [1966], Calculation of potential flow about arbitrary bodies, *Prog. Aeronaut. Sci.* **8**, 1–139.

Sreenath, N., Y. G. Oh, P. S. Krishnaprasad, and J. E. Marsden [1988], The dynamics of coupled planar rigid bodies. Part 1: Reduction, equilibria and stability, *Dyn. Stab. Syst.* **3**, 25–49.

Taylor, G. I. [1952], Analysis of the swimming of long and narrow animals, *Proc. Roy. Soc. London A* **214(1117)**, 158–183.

Tytell, E. D., and G. V. Lauder [2004], The hydrodynamics of eel swimming. I. Wake structure, *J. Exp. Biol.*, **207**, 1825–1841.

Tytell, E. D. [2004], The hydrodynamics of eel swimming. II. Effect of swimming speed, *J. Exp. Biol.*, **207**, 3265–3279.

Webb, P. W. [1991], Composition and mechanics of routine swimming of rainbow trout, *Oncorhynchus mykiss*. *Can. J. Fish. Aquat. Sci.* **48**, 583–590.

Wu, T. Y. [1971], Hydrodynamics of swimming fish and cetaceans, *Adv. Appl. Math.* **11**, 1–63.